ISSN 2531-2189

Volume 6, Issue 18 – July – December - 2022

Journal of Mechanical Engineering

ECORFAN®

Journal of Mechanical Engineering Volume 6, Issue 18, July- December 2022, is a journal edited semestral by ECORFAN-Spain. 38 Matacerquillas, Moralzarzal - CP-28411. Madrid - Spain. WEB: www.ecorfan.org/spain, revista@ecorfan.org. Editor in Chief: SERRUDO-GONZALES, Javier. BsC. ISSN-2531-2189. Responsible for the latest update of this number ECORFAN Computer Unit. ESCAMILLA-BOUCHÁN, Imelda. PhD, LUNA-SOTO, Vladimir. PhD. 38 Matacerquillas, Moralzarzal - CP-28411. Madrid - Spain, last updated December 31, 2022.

Journal of Mechanical Engineering

Definition of Research Journal

Scientific Objectives

Support the international scientific community in its written production Science, Technology and Innovation in the Field of Engineering and Technology, in Subdisciplines of pumps and equipment for handling liquids, bearings, air compressors, gears, cooling equipment, mechanical power transmission equipment, pneumatic equipment, equipment and industrial machinery, agricultural machinery, oil extraction machinery, printing and reproduction machinery, mining machinery, hydraulic machinery, specialized industrial machinery, nuclear machinery, paper making machinery, machinery for the food industry, machinery for material handling, textile machinery, steam machinery, vending machines and distributors, machines, tools and accessories , heating material, construction material, dies, templates and gauges, internal combustion engines (general), gas engines, mechanized operations.

ECORFAN-Mexico SC is a Scientific and Technological Company in contribution to the Human Resource training focused on the continuity in the critical analysis of International Research and is attached to CONACYT-RENIECYT number 1702902, its commitment is to disseminate research and contributions of the International Scientific Community, academic institutions, agencies and entities of the public and private sectors and contribute to the linking of researchers who carry out scientific activities, technological developments and training of specialized human resources with governments, companies and social organizations.

Encourage the interlocution of the International Scientific Community with other Study Centers in Mexico and abroad and promote a wide incorporation of academics, specialists and researchers to the publication in Science Structures of Autonomous Universities - State Public Universities - Federal IES - Polytechnic Universities - Technological Universities - Federal Technological Institutes - Normal Schools - Decentralized Technological Institutes - Intercultural Universities - S & T Councils - CONACYT Research Centers.

Scope, Coverage and Audience

Journal of Mechanical Engineering is a Research Journal edited by ECORFAN-Mexico S.C in its Holding with repository in Spain, is a scientific publication arbitrated and indexed with semester periods. It supports a wide range of contents that are evaluated by academic peers by the Double-Blind method, around subjects related to the theory and practice of pumps and equipment for handling liquids, bearings, air compressors, gears, cooling equipment, mechanical power transmission equipment, pneumatic equipment, equipment and industrial machinery, agricultural machinery, oil extraction machinery, printing and reproduction machinery, mining machinery, hydraulic machinery, specialized industrial machinery, nuclear machinery, paper making machinery, machinery for the food industry, machinery for material handling, textile machinery, steam machinery, vending machines and distributors, machines, tools and accessories , heating material, construction material, dies, templates and gauges, internal combustion engines (general), gas engines, mechanized operations with diverse approaches and perspectives, that contribute to the diffusion of the development of Science Technology and Innovation that allow the arguments related to the decision making and influence in the formulation of international policies in the Field of Engineering and Technology. The editorial horizon of ECORFAN-Mexico® extends beyond the academy and integrates other segments of research and analysis outside the scope, as long as they meet the requirements of rigorous argumentative and scientific, as well as addressing issues of general and current interest of the International Scientific Society.

Editorial Board

Arbitration Committee

Assignment of Rights

The sending of an Article to Journal of Mechanical Engineering emanates the commitment of the author not to submit it simultaneously to the consideration of other series publications for it must complement the Originality Format for its Article.

The authors sign the Authorization Format for their Article to be disseminated by means that ECORFAN-Mexico, S.C. In its Holding Spain considers pertinent for disclosure and diffusion of its Article its Rights of Work.

Declaration of Authorship

Indicate the Name of Author and Coauthors at most in the participation of the Article and indicate in extensive the Institutional Affiliation indicating the Department.

Identify the Name of Author and Coauthors at most with the CVU Scholarship Number-PNPC or SNI-CONACYT- Indicating the Researcher Level and their Google Scholar Profile to verify their Citation Level and H index.

Identify the Name of Author and Coauthors at most in the Science and Technology Profiles widely accepted by the International Scientific Community ORC ID - Researcher ID Thomson - arXiv Author ID - PubMed Author ID - Open ID respectively.

Indicate the contact for correspondence to the Author (Mail and Telephone) and indicate the Researcher who contributes as the first Author of the Article.

Plagiarism Detection

All Articles will be tested by plagiarism software PLAGSCAN if a plagiarism level is detected Positive will not be sent to arbitration and will be rescinded of the reception of the Article notifying the Authors responsible, claiming that academic plagiarism is criminalized in the Penal Code.

Arbitration Process

All Articles will be evaluated by academic peers by the Double Blind method, the Arbitration Approval is a requirement for the Editorial Board to make a final decision that will be final in all cases. MARVID® is a derivative brand of ECORFAN® specialized in providing the expert evaluators all of them with Doctorate degree and distinction of International Researchers in the respective Councils of Science and Technology the counterpart of CONACYT for the chapters of America-Europe-Asia- Africa and Oceania. The identification of the authorship should only appear on a first removable page, in order to ensure that the Arbitration process is anonymous and covers the following stages: Identification of the Research Journal with its author occupation rate - Identification of Authors and Coauthors - Detection of plagiarism PLAGSCAN - Review of Formats of Authorization and Originality-Allocation to the Editorial Board- Allocation of the pair of Expert Arbitrators-Notification of Arbitration -Declaration of observations to the Author-Verification of Article Modified for Editing-Publication.

Instructions for Scientific, Technological and Innovation Publication

Knowledge Area

The works must be unpublished and refer to topics of pumps and equipment for handling liquids, bearings, air compressors, gears, cooling equipment, mechanical power transmission equipment, pneumatic equipment, equipment and industrial machinery, agricultural machinery, oil extraction machinery, printing and reproduction machinery, mining machinery, hydraulic machinery, specialized industrial machinery, nuclear machinery, paper making machinery, machinery for the food industry, machinery for material handling, textile machinery, steam machinery, vending machines and distributors, machines, tools and accessories , heating material, construction material, dies, templates and gauges, internal combustion engines (general), gas engines, mechanized operations and other topics related to Engineering and Technology.

Presentation of the Content

In the first chapter we present, *Behavior analysis of a hydraulic circuit through a low-cost data acquisition system* by CERVANTES-ÁLVAREZ, Francisco Andrés, LÓPEZ-OLMOS, Fabrizio, TORRES-DEL CARMEN, Felipe de Jesús and CAPILLA-GONZÁLEZ, Gustavo, with adscription in the Universidad de Guanajuato, as next article we present, *Determination of Physical parameters that contribute to the erosion of rotor blades in a steam turbine* by RUEDA-MARTINEZ, Fernando, GARRIDO-MELÉNDEZ, Javier, MENDOZA-GONZÁLEZ, Felipe and RODRÍGUEZ-GARCÍA, Ernesto R., with adscription in the Universidad Veracruzana, as next article we present, *Characterization of the relationship soil density and simple compression resistance of silty soils* by RUIZ-CHÁVEZ, Felipe de Jesús, GUTIÉRREZ-VILLALOBOS, José Marcelino and ARROYO, Hiram, with adscription in the Universidad de Guanajuato, as the last article we present, *Design and manufacture of a splint prototype for the upper extremities of the human body* by LICONA-GONZALEZ, Marlon, IBARRA-ROBLES, Gabriel Ted, MENTLE-GALINDO, Margarita and BLAS-SANCHEZ, Luis Ángel, with adscription in the Universidad Tecnológica de Xicotepec de Juárez.

Content

Article	Page
Behavior analysis of a hydraulic circuit through a low-cost data acquisition system CERVANTES-ÁLVAREZ, Francisco Andrés, LÓPEZ-OLMOS, Fabrizio, TORRES-DEL CARMEN, Felipe de Jesús and CAPILLA-GONZÁLEZ, Gustavo *Universidad de Guanajuato*	1-7
Determination of Physical parameters that contribute to the erosion of rotor blades in a steam turbine RUEDA-MARTINEZ, Fernando, GARRIDO-MELÉNDEZ, Javier, MENDOZA-GONZÁLEZ, Felipe and RODRÍGUEZ-GARCÍA, Ernesto R. *Universidad Veracruzana*	8-14
Characterization of the relationship soil density and simple compression resistance of silty soils RUIZ-CHÁVEZ, Felipe de Jesús, GUTIÉRREZ-VILLALOBOS, José Marcelino and ARROYO, Hiram *Universidad de Guanajuato*	15-20
Design and manufacture of a splint prototype for the upper extremities of the human body LICONA-GONZALEZ, Marlon, IBARRA-ROBLES, Gabriel Ted, MENTLE-GALINDO, Margarita and BLAS-SANCHEZ, Luis Ángel *Universidad Tecnológica de Xicotepec de Juárez*	21-28

Article **Journal of Mechanical Engineering**
December, 2022 Vol.6 No.18 1-7

Behavior analysis of a hydraulic circuit through a low-cost data acquisition system

Análisis del comportamiento de un circuito hidráulico a través de un sistema de adquisición de datos de bajo costo

CERVANTES-ÁLVAREZ, Francisco Andrés†, LÓPEZ-OLMOS, Fabrizio, TORRES-DEL CARMEN, Felipe de Jesús* and CAPILLA-GONZÁLEZ, Gustavo

Universidad de Guanajuato, División de Ingenierías Campus Irapuato-Salamanca, Departamento de Ingeniería Mecánica

ID 1st Author: *Francisco Andrés, Cervantes-Álvarez* / **ORC ID**: 0000-0002-8026-3788, **Researcher ID Thomson**: GQO-7474-2022, **CVU CONACYT ID**: 1105037

ID 1st Co-author: *Fabrizio, López-Olmos* / **ORC ID**: 0000-0001-5368-2285, **CVU CONACYT ID**: 1076916

ID 2nd Co-author: *Felipe De Jesús, Torres-Del Carmen* / **ORC ID**: 0000-0001-5792-2098, **CVU CONACYT ID**: 170819

ID 3rd Co-author: *Gustavo, Capilla-González* / **ORC ID**: 0000-0002-6903-2567, **CVU CONACYT ID**: 347519

DOI: 10.35429/JME.2022.18.6.1.7 Received: September 30, 2022; Accepted: December 30, 2022

Abstract

In an industrial process exists several variables to be monitored, in particular, temperature is a main variable for many systems as a hydraulic circuit. Due to friction effects and recirculation of the fluid, a temperature increasing is noted causing some variations on physical properties of the oil. In this work, the design and implementation of a low-cost system is covered for data acquisition of the oil temperature and advance time of the final actuator. This system is composed by a minicomputer Raspberry Pi, a submersible digital sensor and programming code in Python; the hydraulic circuit is built with a hydraulic source equipment, a solenoid valve, a double-acting cylinder and two limit switches. The proposed approach is experimentally proved in a continuous process with 200 iterations for the cylinder to advance and retract, which results in a rising temperature. Furthermore, with available data from the advance time, the effect caused by the temperature on the advance velocity is observed by means of plots of temperature and velocity from the low-cost monitoring system.

Raspberry Pi, Temperature Digital Sensor, Velocity of a Cylinder, Hydraulic Circuit

Resumen

En un proceso industrial existen variables de interés para ser monitoreadas, particularmente la temperatura es fundamental para distintos sistemas como un circuito hidráulico. Debido a la fricción y la recirculación del fluido se nota un incremento de la temperatura, causando efectos sobre las propiedades físicas del aceite. En este trabajo se aborda el diseño e implementación de un sistema de bajo costo a través de una minicomputadora Raspberry Pi, un sensor digital sumergible y programación en Python para la adquisición de datos de la temperatura del aceite que es usado en un circuito hidráulico, el cual está compuesto por un equipo de suministro de potencia hidráulica, una electroválvula, un cilindro de doble efecto y dos sensores de límite de carrera. Se probó experimentalmente el esquema propuesto en un proceso continuo de 200 iteraciones de avance y retroceso del actuador final, en donde se manifiesta un incremento de temperatura del aceite. Más aún, con los datos obtenidos del tiempo de avance, se comprueba el efecto que causa la temperatura del fluido en la velocidad de avance del cilindro de doble efecto, como lo muestran las gráficas del comportamiento de la temperatura y velocidad a partir del sistema de monitoreo de bajo costo.

Raspberry Pi, Sensor Digital de Temperatura, Velocidad de un Cilindro, Circuito Hidráulico

Citation: CERVANTES-ÁLVAREZ, Francisco Andrés, LÓPEZ-OLMOS, Fabrizio, TORRES-DEL CARMEN, Felipe de Jesús and CAPILLA-GONZÁLEZ, Gustavo. Behavior analysis of a hydraulic circuit through a low-cost data acquisition system. Journal of Mechanical Engineering. 2022. 6-17: 1-7

* Correspondence to the Author (e-mail: fdj.torres@ugto.mx)
† Researcher contributing as first author.

Introduction

A hydraulic circuit is made up of various types of elements that handle pressurised oil. Generally speaking, we can identify those elements that supply the hydraulic power, those that capture information, control elements and, finally, the output elements, which are the actuators. Therefore, a hydraulic circuit can be described as a set of a motor-pump unit, filters, pressure regulating valve, relief valve, pressure gauge, stroke limit sensors, directional control valve, which depending on how it is activated, can be considered a solenoid valve if it uses an electromagnet to switch; finally, a double-acting cylinder as an actuator.

The design of hydraulic circuits is a task that allows the automation of industrial processes, based on the displacement-phase diagrams of the final actuators. However, it is important to know the behaviour of certain variables of interest such as oil temperature, due to a potential risk of explosion if the oil rises to a temperature that causes ignition in relation to the working pressure.

In the industrial components market there are sensors that allow temperature monitoring, which are relatively expensive at $2,500.00 MXN and require additional components, resulting in a system that is difficult to access for small and medium sized companies.

On the other hand, the use of frontier computing adds benefits of agility, real-time information processing and autonomy to create value to manufacturing intelligence (Moreno and Victoria, 2009). Thus, one of the most important fronts that has been highlighted in recent years within research and technological development focuses on the use of new low-cost technologies for industrial applications. For example, regarding monitoring through a commercially developed board, Othman *et al*. (2017) implements a low-cost monitoring system through a Raspberry Pi to understand the performance of a low-scale solar PV system. McBride and Courter (2019) use Raspberry Pi minicomputers to monitor a flock of birds and the environmental conditions of the site where they are growing. Sowmya *et al*. (2020) build a Raspberry Pi-based robotic car monitoring system.

Dupont *et al*. (2018) design and implement a photovoltaic water pumping equipment monitoring system, where the Raspberry Pi board is used to develop a Linux embedded system. Hasan (2020) uses the Raspberry Pi to monitor the variables of temperature, humidity, pH and water level of a crop field.

Therefore, in this work the main element for the implementation of monitoring and analysis is the minicomputer on Raspberry Pi (RPi) board, which has the characteristic of being low cost and small dimensions to be considered as a border computing device, in addition the DS18B20 temperature sensor is used, which is capable of immersing in fluids and stroke limit sensors. The Python programming language is used to build a real-time data acquisition system, which is stored in the Raspberry Pi itself, enabling the possibility of being analysed at a later stage of the experiment.

The rest of the article is presented as follows: section 1 details the methodology and the main characteristics of the Raspberry Pi used and the sensor; section 2 describes the procedure for the characterisation of the DS18B20 temperature sensor as well as the main characteristics of the sensor; section 3 shows the results obtained from the experimental tests; section 4 analyses the data and, finally, section 5 includes the conclusions of the work presented and future work.

1. Metodology

The test bench used for the characterisation of the temperature sensor is the one located at the University of Guanajuato, Engineering Division, Irapuato-Salamanca Campus, which is a hydraulic circuit with the typical components used in an industrial process, shown in Figure 1.

ISSN-2531-2189

CERVANTES-ÁLVAREZ, Francisco Andrés, LÓPEZ-OLMOS, Fabrizio, TORRES-DEL CARMEN, Felipe de Jesús and CAPILLA-GONZÁLEZ, Gustavo. Behavior analysis of a hydraulic circuit through a low-cost data acquisition system. Journal of Mechanical Engineering. 2022

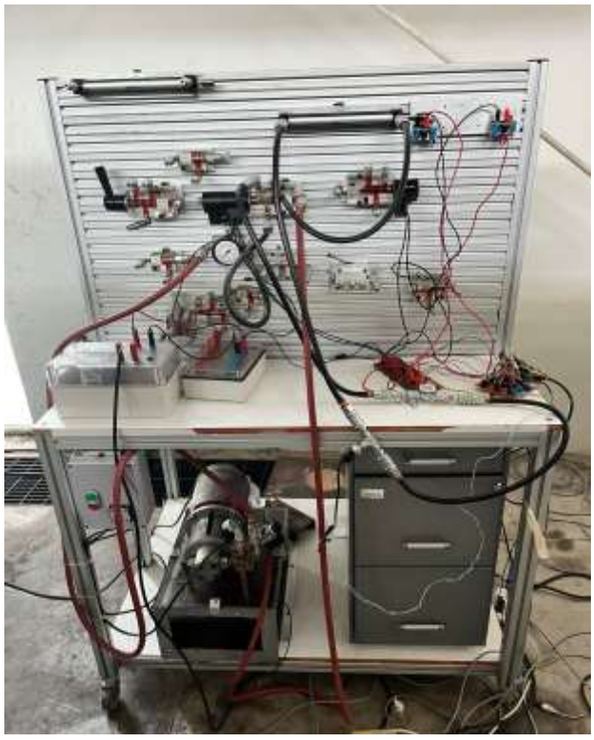

Figure 1 Test bench
Source Own Elaboration

In this process, a Raspberry Pi is used as a means of data acquisition where the Python programming language is used to obtain the measurements made by the DS18B20 temperature sensor and the stroke limit sensors, in order to be able to analyse the results obtained. The main characteristics of both the Raspberry Pi and the DS18B20 temperature sensor are described below.

1.1 Raspberry Pi 2 model B

This model was launched in 2014 and is shown in Figure 2, with 1GB of RAM. It includes 40 GPIO pins and four USB ports.

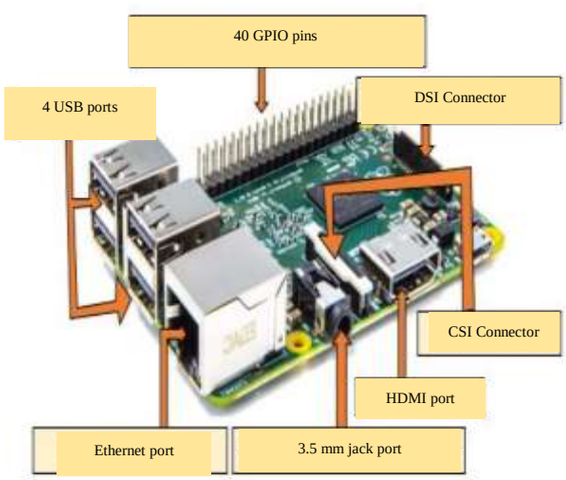

Figure 2 Parts of the RPi model 2B (Kumar and Pati, 2016)

This model has the following specifications:

– Processor: 900 MHz Broadcom BCM2836 quad core ARM quad core Cortex-A7 quad core.
– GPU: Dual-core VideoCore IV with Open GL ES 2.0 support, hardware accelerated OpenVG up to 1080p30 H.264.
– RAM: 1GB SDRAM LPDDR2.
– WiFi connection: No WiFi connection.
– Serial communication ports: UART, RXD and TXD (support I2C and SPI protocols).
– ADC converter: It does not have its own converter, so it is necessary to implement an external one.
– Ethernet connection: This model reaches a maximum speed of 100 Mbit/s.
– Operating system: Raspbian.

1.2 RPi configuration

As it is a minicomputer, the first configuration carried out on the RPi was the installation of an operating system. For this work, the operating system recommended by the RPi organisation was installed, which is called Rasbian, which is a variation of Debian. This system works on the basis of Linux and is also free to use. For this, it was only necessary to boot a micro SD memory, which also acts as the main hard disk of the RPi. In this work, a 64 Gb SD memory is used. Once the operating system is installed, we proceed to install some tools that do not come by default in Raspbian, such as Phyton and its IDLE Thonny.

1.2 Characteristics of the Temperature Sensor DS18B20

To read the temperature of the system, we use the DS18B20 sensor which is low cost (about $45.50 MXN), capable of immersion in fluids and is shown in Figure 3.

The sensor has the following features:

– Requires only one port pin for communication
– Supply voltage range: 3.0V to 5.0VDC
– Measuring range: -55°C to 125°C
– 9 to 12 bit readings (configurable)
– Connection via One Wire protocol.

ISSN-2531-2189

Figure 3 Temperature sensor DS18B20

1.4 Stroke limit sensor

Low-cost limit switches are also mechanical switches that are activated by means of a roller, which is actuated through contact with the cylinder. These limit switches can be positioned at the start or end of the stroke of a hydraulic cylinder or at any position the user deems appropriate. In such a way that the distance between the stroke limit sensors is considered constant, therefore, and taking into account the mathematical equation that defines the velocity, which relates the change in the displacement with respect to a change in the time in which it is made, it is possible to measure the advance speed of the cylinder if the reading of the activation time between the sensor at the start of the stroke and the one at the end of the stroke is obtained.

In this way, the sensors are fixedly positioned to keep the distance between them constant and thus the change in the advance displacement of the double-acting cylinder.

Validation of the DS18B20 sensor

The temperature sensor DS18B20 is immersed in the oil tank to determine its temperature during the process, while the stroke limit sensors are positioned within the range of the displacement of the double-acting cylinder, maintaining a constant distance between them, as shown in Figure 4.

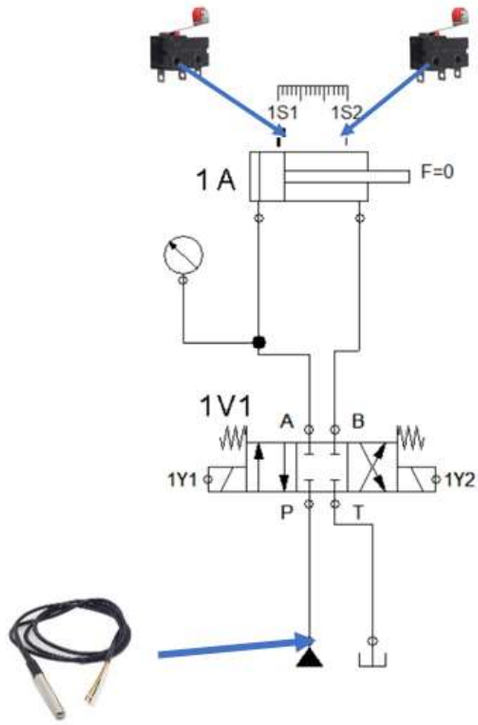

Figure 4 Hydraulic circuit assembled with the DS18B20 temperature sensor and limit sensors
Source: Own Elaboration

For the validation of the temperature sensor, a Steren MUL-115 multimeter is used. This multimeter has the characteristics of measuring temperature in the range of -20 to 150°C±(3°C+1d)/150 to 1000°C±(3%+2d) according to the data sheet provided by the distributor.

For the measurement of the oil temperature it was decided to place the sensor inside the oil tank as well as the multimeter as shown in Figure 5.

Figure 5 Measurement of the fluid inside the tank with the multimeter
Source: Own Elaboration

ISSN-2531-2189

It allows the temperature of the fluid to be analysed before it is pumped into the system, measuring the thermal equilibrium that is reached when the oil re-enters the tank after the process has been completed. The multimeter is used to measure the temperature within the same point in the tank as the temperature sensor, however, the measurement obtained by the multimeter only has integer values within the range specified by the distributor data sheet. In order to increase the fluid temperature more rapidly, an electrical resistor is introduced into the tank to heat the oil and take measurements every 15 seconds for 5 minutes and thus, with a total of 30 measurements, calibrate the DS18B20 sensor through a linear regression model.

Using the least squares regression methodology, the following equations are obtained:

$$\hat{b} = \frac{\sum x_i y_i - n x_m y_m}{\sum x_i^2 - n x_m^2} \quad (1)$$

$$\hat{a} = \frac{\sum y_i - \hat{b}\sum x_i}{n} = y_m - \hat{b} x_m \quad (2)$$

where x_i are the values obtained from the multimeter, y_i are the values obtained from the sensor, n is the number of data, x_m, y_m are the averages of the multimeter and sensor data, respectively. This gives the linear regression model described in equation:

$$y = \hat{a} + \hat{b}x \quad (3)$$

The results obtained by the DS18B20 temperature sensor and the Steren MUL-115 multimeter, before applying the linear regression, are presented in Figure 1.

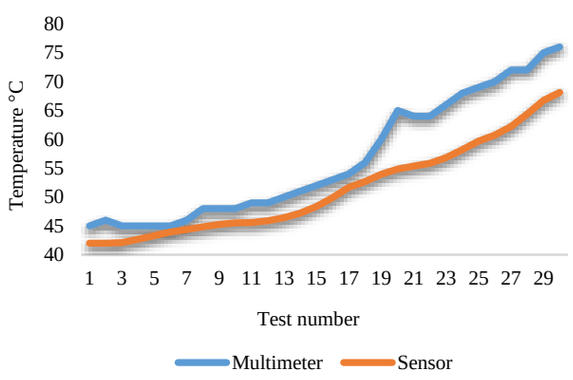

Graph 1 Temperature measurements, comparison between multimeter and sensor
Source: Own Elaboration

The results obtained with the implementation of the linear regression equation are shown in Figure 2.

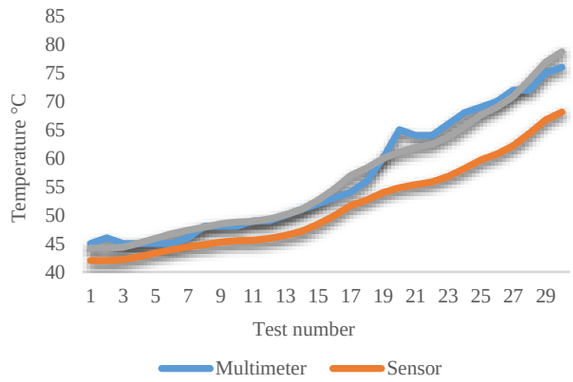

Graph 2 Regression model on sensor measurements
Source: Own Elaboration

1.5 Circuit assembly RPi

For the assembly of the circuit with the RPi, the pins shown in Table 1 were selected.

Pin	Description
3V3	Power supply used throughout the RPi circuit at 3.3 Volts DC
PIN GROUND	Grounding throughout the RPi circuit
GPIO 2	Connection to temperature sensor data cable DS18B20
GPIO 6	Connection to the start of stroke sensor
GPIO 12	Connection to end-of-stroke sensor

Table 1 Description of the connections of the RPi

2. Experimental results

In the manufacturing laboratory of the Division of Engineering of the Irapuato Salamanca Campus of the University of Guanajuato there is a hydraulic circuit test bench with which the physical implementation of the proposed approach was carried out in order to obtain experimental results.

Hydraulic power supply equipment, a double solenoid solenoid valve and a double acting cylinder were used, interconnecting each of the components through hydraulic hoses. As part of the instrumentation, the DS18B20 sensor submerged in the oil tank or reservoir and the start and end of stroke roller sensors in the cylinder stroke were used; all of them connected to the RPi for the data acquisition system.

ISSN-2531-2189

The experimentation was done in a continuous process with 200 iterations of forward and reverse of the double-acting cylinder. In addition, 4 temperature measurements were considered for each advance. In total, 800 measurements were taken. At each advance an average of the 4 respective measurements was taken. The results of the oil temperature during the 200 iterations are shown in Figure 6.

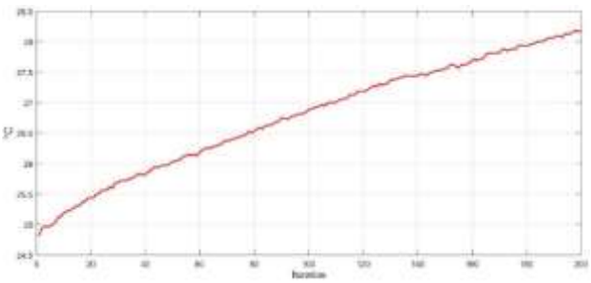

Figure 6 Results obtained from the measurement of oil temperature during 200 continuous iterations
Source: Own Elaboration

The advance time of the hydraulic cylinder in each iteration was calculated as follows. The RPi processor time is taken when the activation of the start-of-stroke sensor is detected and stored in a variable. When the activation of the end-of-stroke sensor is detected, the RPi time is taken again and stored in another variable. A difference of the end-of-stroke time minus the start-of-stroke time is made to know the advance time. The results are shown in Figure 7.

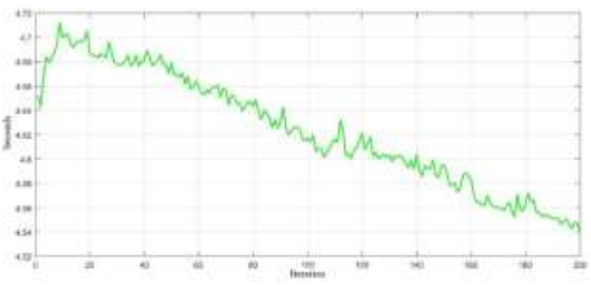

Figure 7 Hydraulic cylinder advance time for 200 continuous iterations
Source: Own Elaboration

The distance between the limit switches is a constant quantity with a value of 15.6 cm, as shown in Figure 8.

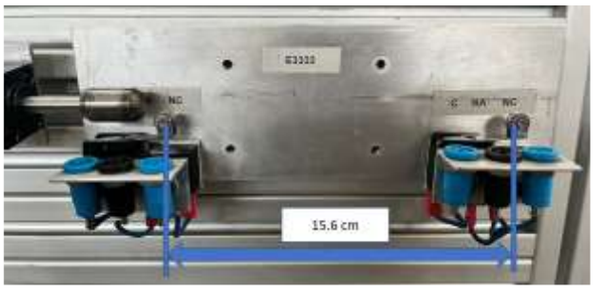

Figure 8 Fixed distance between the stroke limit sensors

It is possible to calculate the forward speed, using the equation:

$$\text{forward speed} = \frac{scrolling}{time\ of\ advance} \quad (3)$$

The results of the 200 continuous iterations are given in Figure 9.

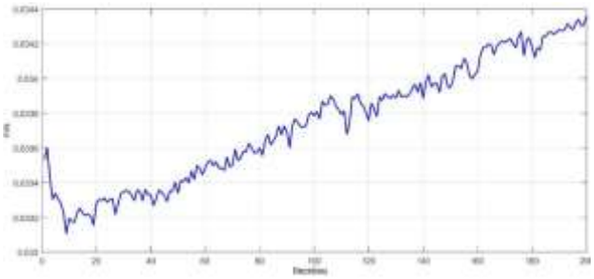

Figure 9 Results of the feed rate of the hydraulic cylinder during 200 continuous iterations
Source: Own Elaboration

3. Analysis of the data obtained

The oil temperature increased during the 200 continuous forward and reverse iterations of the double-acting cylinder, probably due to the effects of friction and fluid recirculation. It is important to note that no heating devices were used during the experimental tests. Also, no components were used to cool the oil during its flow through the hydraulic circuit.

The oil used in the hydraulic circuit is synthetic oil for automatic transmission, which has the physical properties given in Table 2.

Property	Value
Viscosity @ 100°C, cSt	7.5
Viscosity @ 40°C, cSt	34.0
Pour point, °C	-60
Flash point, °C	249

Table 2 Properties of synthetic oil used in the hydraulic circuit
Source: Own Elaboration

ISSN-2531-2189

It is understood that increasing temperature affects the viscosity of the oil. Moreover, according to Wang (2014), the increase in temperature causes the fluid to flow faster. Therefore, the velocity is increased, as proven by the results of the forward speed of the hydraulic cylinder.

The analysis carried out shows that it is important to consider the effects of temperature on the oil in a hydraulic circuit when it is necessary to maintain the advance speed or, directly related, the advance time of the final actuator. Since, in sequential industrial automation processes, the times in each of the stages of the process are important to keep fixed. Therefore, the relevance of heat exchangers in the oil recirculation path in a hydraulic circuit and the continuous monitoring of the temperature as a variable of great interest for the correct operation of the industrial process.

Conclusions

It has been possible to build a low-cost data acquisition system using an RPi minicomputer, in addition to obtaining a characterisation of the DS18B20 temperature sensor with a percentage error between the regression model and the readings obtained by the temperature sensor of ±1.8%. The advance time of the double-acting cylinder in a real hydraulic circuit is also monitored.

The experimental tests yield relevant data to understand the behaviour of the fluid in a continuous process of several iterations. The analysis of the data demonstrates the importance of oil cooling for sequential automation applications where constant cylinder advance times are guaranteed.

Future work will consider including a larger number of sensors to measure other variables of interest that are related to the change in fluid properties such as flow rate.

References

Dupont, I., Pereira, R., Juca, S., y Carvalho, P. (2018). Internet of Things Data acquisition system applied to photovoltaic water pumping. *IEEE Latin America Transactions*, 16(10), 2547-2560.

Hasan, M. (2020). Real-time and low-cost IoT based farming using raspberry Pi. *Indonesian Journal of Electrical Engineering and Computer Science*, 17(1), 197-204.

Kumar, P., y Pati, U. C. (2016, November). Arduino and Raspberry Pi based smart communication and control of home appliance system. *In 2016 Online International Conference on Green Engineering and Technologies (IC-GET)* (pp. 1-6). IEEE.

McBride, W. J., y Courter, J. R. (2019). Using Raspberry Pi microcomputers to remotely monitor birds and collect environmental data. *Ecological Informatics*, 54, 101016.

Othman, N. A., Zainodin, M. R., Anuar, N., y Damanhuri, N. S. (2017, November). Remote monitoring system development via Raspberry-Pi for small scale standalone PV plant. *In 2017 7th IEEE International Conference on Control System, Computing and Engineering (ICCSCE)* (pp. 360-365). IEEE.

Sowmya, K. V., Jamedar, H., y Godavarthi, P. (2020). Remote Monitoring System of Robotic Car Based on Internet of Things Using Raspberry Pi. *Journal of Computational and Theoretical Nanoscience*, 17(5), 2288-2295

Wang, C., Liu, S., Wu, J., y Li, Z. (2014). Effects of temperature-dependent viscosity on fluid flow and heat transfer in a helical rectangular duct with a finite pitch. *Brazilian Journal of Chemical Engineering*, 31, 787-797.

ISSN-2531-2189

Article **Journal of Mechanical Engineering**
December, 2022 Vol.6 No.18 8-14

Determination of Physical parameters that contribute to the erosion of rotor blades in a steam turbine

Determinación de parámetros Físicos que contribuyen en la erosión de álabes rotores en una turbina de vapor

RUEDA-MARTINEZ, Fernando†, GARRIDO-MELÉNDEZ, Javier, MENDOZA-GONZÁLEZ, Felipe* and RODRÍGUEZ-GARCÍA, Ernesto R.

Universidad Veracruzana, Facultad de Ingeniería región Coatzacoalcos, México

ID 1st Author: *Fernando, Rueda-Martínez* / **ORC ID:** 0000-0002-6144-0996, **arXiv Author ID:** frueda, **CVU CONACYT ID:** 167238

ID 1st Co-author: *Javier, Garrido-Meléndez* / **ORC ID**: 0000-0001-9143-408X, **Researcher ID Thomson**: C-9373-2018, **CVU CONACYT ID**: 101615

ID 2nd Co-author: *Felipe, Mendoza-González* / **ORC ID:** 0000-0003-1172-6782, **Researcher ID Thomson:** S-6747-2018, **CVU CONACYT ID:** 947336

ID 3rd Co-author: *Ernesto Raúl, Rodríguez-García* / **ORC ID:** 0000-0001-6239-1797, **CVU CONACYT ID:** 597318, **arXiv Author ID:** ErnestoRaul

DOI: 10.35429/JME.2022.18.6.8.14 Received: September 30, 2022; Accepted: December 30, 2022

Abstract

The last rotor blades of the steam turbines in their low pressure section, work the steam with humidity. The combination of its high velocities with the existence of liquid microparticles presents a repeated impact on its surface, which will cause losses in the aerodynamic characteristics in the passage section, affecting its performance. This study evaluates the influence exerted by different physical parameters, such as the frequency of impacts, size of the drops that cause damage, impulse pressure, etc., on the erosion shown by the blades in the last stage of the low pressure section in a steam turbine under operating conditions equal to design.

Steam Turbine, Erosion, Droplets

Resumen

Los últimos álabes rotores de las turbinas de vapor en su sección de baja presión, trabajan el vapor con humedad. La combinación de sus altas velocidades con la existencia de micropartículas líquidas presenta un impacto repetido sobre su superficie, lo que causará pérdidas en las características aerodinámicas en la sección de paso, afectando su rendimiento. En este estudio se evalúa la influencia que ejercen diferentes parámetros físicos, como la frecuencia de impactos, dimensión de las gotas que causan daño, presión de impulso, etc., sobre la erosión que demuestran los álabes en el último paso de la sección de baja presión en una turbina de vapor en condiciones de operación iguales a las de diseño.

Turbina de Vapor, Erosión, Gotas

Citation: RUEDA-MARTINEZ, Fernando, GARRIDO-MELÉNDEZ, Javier, MENDOZA-GONZÁLEZ, Felipe and RODRÍGUEZ-GARCÍA, Ernesto R. Determination of Physical parameters that contribute to the erosion of rotor blades in a steam turbine. Journal of Mechanical Engineering. 2022. 6-18: 8-14

* Correspondence to the Author (e-mail: femendoza@uv.mx)
† Researcher contributing as first author.

Introduction

The determination of the different parameters that influence erosion in steam turbines is carried out to learn more about the cause that causes their wear, and to have more information about the problems of mechanical erosion. The dependence of the erosion of the blades on the variables of the steam is complicated, due to the microparticles of liquid and the different operating conditions that must be maintained. The analyzed turbine has a power of 300 MW, operating at 3600 rpm.

1. Moisture Formation

A characteristic singularity of steam expansion in some turbine elements is the fact that during the transition from one-phase to two-phase region of state in converging (accelerating) flows with high velocities and large gradients absolute values of pressure, the variation of the thermodynamic parameters occurs so fast that the condensation equilibrium process does not take place. The steam temperature turns out to be below the corresponding saturation temperature (supercooling, see fig. 1).

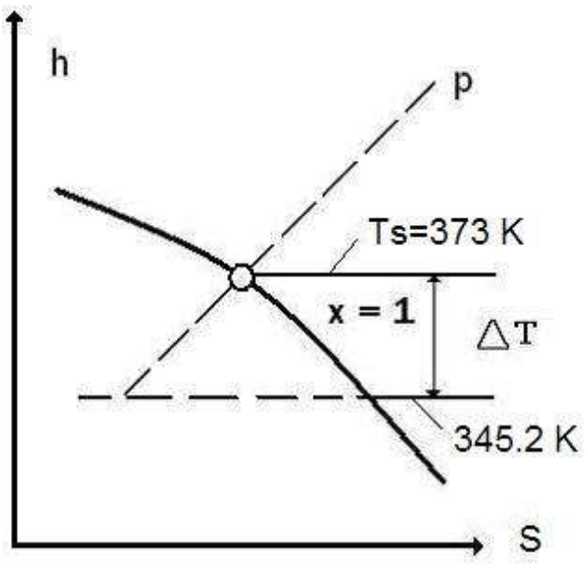

Figure 1 Determination of the equilibrium state of supercooling of steam from the h, s diagram

Upon reaching maximum local supercooling, the vapor spontaneously passes to a state that is close to equilibrium. The new phase arises in the form of very small droplets that are the condensation nuclei. In the process of expansion on these nuclei, condensation of the surrounding vapor takes place. The emergence of the new phase occurs as a result of the collision of molecules.

During the chaotic movement there are always molecules with velocities and energies that differ from the average values, leaving the limits of an aggregation state. The deviations of very small drops (composed of several molecules) are unstable, and only germs, whose dimension exceeds the critical one, are viable. Further growth of the new phase takes place on these stable formations called condensation nuclei. The magnitude of the radius of the critical germ (Troyanovsky, 1987), suitable for further growth, is determined from the equilibrium condition of the biphasic medium: steam and water droplets. The increase in supercooling of the steam leads to a reduction in the critical radius of the seed and to an intensification of the nuclei formation process. The number of nuclei that arise begins to be considerable that an impetuous condensation of steam begins on them. In the center of the vortices that break off from the trailing edge of the rotor blade profile there is a zone of low temperature. The supercooled vapor, upon reaching this zone, intensely condenses, and the drops that form are expelled from the vortex to the core of the flow.

The humidity at the entrance of the crown has different concentration and different degree of dispersion, while the velocities of the humidity droplets differ from the velocity of the vapor, both for their magnitude and for their direction. The trajectories of the moisture droplets (see fig. 2) can be different, losing their stability and breaking up. The small droplets follow the streamlines of the main flow; its velocity by magnitude and direction differs little from that of steam.

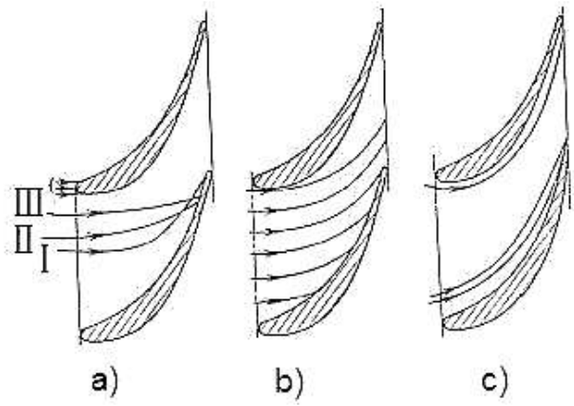

Figure 2. Trajectory of the water drops in the channel of the stator blade crown. a, drops of different dimensions at the entrance: I, with $d_d = 2\mu m$; II, with $d_g = 20\mu m$; III, with $d_g = 200\mu m$; b, drops of equal dimensions at the entrance with $d_g = 10\mu m$; c, drops of equal dimensions at the entrance with $d_g < 1\mu m$ (Schegliáiev)

ISSN-2531-2189

An important characteristic of the biphasic medium is the slip coefficient (Troyanovsky, 1987), that is, the ratio between the velocities of the liquid phase (moisture particles) and that of the vapor phase. If the drops are larger, the slip coefficient will be lower. Due to this sliding between the phases, the mechanical action of large droplets in the vapor flow is of great importance.

In the low pressure section, a decrease in quality occurs, beginning with values without greater risk, until reaching a very low quality of 86% in the last step, which indicates a clear considerable presence of moisture. The blades, when working with this wet steam, suffer the constant action of the collision of the liquid particles, as a result of which wear (erosion) is possible on their surface, and also on other elements of the turbine. The considerable humidity of the steam, in combination with the speeds of the blades, especially the last, is a factor that influences the manifestation of erosion problems.

The geometric parameters of the turbine have a direct influence on the level of erosion, since the design of the blades (height, chord, pitch, entry and exit angles of the profile, warping angle, etc.) directly affects the velocities that operate in the turbomachine.

Special care must be taken in condensing turbines, in the blades that are in the sections of increasing humidity, because, in unfavorable conditions of water content, peripheral speed and geometric configuration, the water droplets that are formed erode the moving blades, wearing away the metal of the leading edges. The water deposited on the stator blades is entrained by the steam flow towards the trailing edge, where it collects to form large droplets. When released from the trailing edge, these droplets, which are about 1 mm in diameter, break up to form smaller droplets (Heinz, 1996). The rotor blades collide with the small droplets and the resulting impact dislodges material from them.

There are many relationships to be able to determine the factors that act on the erosional wear of the leading edges of the blades, so the evaluation of the influence of the different thermodynamic and design parameters can help to understand its causes and to have more precise information about this technological problem.

2. Analysis of Conditions of the Low Pressure Section

Next, relationships are indicated in calculation of the parameters present in mechanical erosion. As mentioned above, the critical seed is capable of increasing the growth of the liquid phase in the vapor flow, only being affected by local supercooling. Thus, according to the pressure and temperature conditions in the 5th stage of the low pressure section, it is observed that the supercooling is 28 K, as seen in fig. 1. Being the radius of the critical germ, it can be calculated from the following equation:

$$r* = \frac{2\sigma T_s}{L\Delta T\rho'}, \tag{1}$$

where σ is the coefficient of surface tension, L is the latent heat of phase transitions, ρ_{liq} is the density of the liquid phase, T_S is the local saturation temperature in the 5th stage and T is the temperature in the 5th stage. From (1), the value of the critical radius is $r* = 3{,}578x10^{-4}\,\mu m$, from which the subsequent growth of the phase begins.

Macrodisperse moisture (Troyanovsky, 1987), whose approximate equation is:

$$\lambda = 0.07 z_{hum} k_{aer} (0.5 - 0.094 \ln p_2), \tag{2}$$

it is the moisture that moves with great slip with respect to the vapor phase. The diameter of the droplets exceeds the diameter of the particles d_{crit} moving in the accelerated flow with sliding $v = c'/c'' \leq 0.8$.

Starting from the pressure in front of the 5th stage, from the value of the improvement constant of the fixed part k_{aer}, and from z_{hum}, number of the stage counting by the one in which the humidity was formed, it was possible to determine that the macrodisperse humidity has a value of 0.2015, which indicates that while decreasing λ, the pressure increases.

The slip coefficient (Troyanovsky, 1987) is obtained through the blade geometry design data, as shown below:

$$v = 15 \cdot 10^{-5} p_1 \frac{u_{per}}{x_{per}} \sqrt{\frac{(\delta_{ax}^{per} + 0.05)}{sen\alpha_1'}(1 - \rho_{per})}, \tag{3}$$

ISSN-2531-2189

where $x_{per} = u_{per} / c_{per}$ is the velocity ratio, ρ_{per} is the degree of reaction near the periphery of the stage, φ is the velocity coefficient, δ_{ax}^{per} is the axial distance between the stator and rotor blades, p_1 is the pressure in the axial set (in kPa), u_{per} is the circular velocity, α is the stator blade outlet angle, where the index "per" refers to the peripheral section. From the characteristics of the stator blade 980BE17° and rotor blade 1182GAx in the 5th stage of the low pressure turbine, it is possible to find the velocities ratio x_{per} which is approximately 0.8115, with a degree of reaction in the periphery of 0.67 based on the hub/tip ratio, according to radial balance theory (Zurita, 1996). Therefore, from (3), the slip coefficient is $v = 0.747$, indicates that the droplets are of regular size, with a diameter that can be d_{crit} .

The velocity $w_{per}^{'}$ (Troyanovsky, 1987) is the relative velocity of the moisture droplets, which becomes the impact velocity at the contact of the drop against the peripheral zone of the rotor blades, this being:

$$(w_{1\ per}^{'})^2 = u_{per}^2 \left[1 + \frac{v^2 \varphi^2 (1-\rho_{per})}{x_{per}^2} - \frac{2v\varphi \cos\alpha_1^{'}}{x_{per}} \sqrt{1-\rho_{per}} \right] \quad (4)$$

and according to the data obtained, and from the design data it can be seen that $w_{per}^{'} \approx 290 m/s$ is a lower value, but it will influence the different stages of contact velocities of the droplet against the blade surface.

The impulse pressure is the local pressure growth during the impact of an (isolated) droplet against the hard surface of the blade, and according to the following equation (Troyanovsky, 1987), the impulse pressure will be equal to the Zhukovsky equation:

$$\Delta p = a^{'} w \rho_{liq}, \quad (6)$$

where $a^{'}$ is the velocity of propagation of the shock wave in the liquid (in a first approximation it can be accepted equal to the speed of sound propagation in the liquid), is the impact velocity of the drop against the surface and ρ_{liq} is the density of the liquid.

According to the nominal value of the pressure in the 5th stage, the velocity $a^{'}$ is about 425 m/s, therefore, the impulse pressure will be equal to $\Delta p \approx 120.5$ MPa. At considerable impact velocities, the driving pressure of the droplet can exceed the metal yield strength and produce residual deformation at the surface. However, it has been experimentally determined that even at lower impact velocities erosional wear occurs, due to fatigue rupture of the surface layers by the action of multiple droplet impacts. Under the action of the impacts delivered, an accumulation of damage takes place on the surface layer that becomes fatigue cracks, which serve as stress concentrators and subsequently lead to the destruction of isolated areas and the deterioration of the metal of the blades

It remains to be noted that the impulse pressure may also depend on a series of additional factors, such as the elasticity of the metal, the shape of the drop, the surface of the metal, etc. The physical parameters proposed here are formed by semi-empirical equations, obtained experimentally. The mean radius of macrodisperse moisture droplets (Troyanovsky, 1987) can be calculated from the mean dimension of macrodisperse moisture droplets using the critical Weber number as the stability characteristic:

$$We = d_{got} (c^{''})^2 / \sigma \upsilon^{''}, \quad (7)$$

And being We = 15 critical, we then have:

$$r_{got} = \frac{15\sigma v_1}{2c_1^2} = \frac{15\sigma \upsilon^{'} x_{per}^2}{2\varphi^2 (1-\rho_{per}) u_{per}^2}, \quad (8)$$

From the data already calculated it is found that the average dimension of the drops is $r_{got} \approx 4\mu m$, therefore it is observed that its diameter is very large, and its trajectory deviates a little from the current lines, as can be seen in fig. 2. The volume of macrodisperse moisture droplets (Troyanovsky, 1987) is obtained from a simple equation:

$$V_{got} = \frac{4\pi}{3} r_{got}^3, \quad (9)$$

being its volume $V_{got} \approx 2.68x10^{-10} \mu m$.

The consumption of the liquid phase in the peripheral zone (Troyanovsky, 1987) can be calculated from the relationship:

$$\Delta G^{'} = O_1 \Delta l z_{p.e.} \frac{c_1}{v_1} = O_1 l_1 z_{p.e.} \frac{u_{per}}{x_{per}} \sqrt{\frac{1-\rho_{per}}{v}} \qquad (10)$$

This equation includes design data, since it is necessary to know O_1 which is the throat of the stator blade, l_1 the length of the stator blade, $z_{p.e.}$ is the number of stator blades. For the turbine in question, the consumption of the liquid phase in the 5th stage was $\Delta G^{'} = 707.7$ m^3/s. The number of large drops per unit of time (Troyanovsky, 1987) is obtained from:

$$Z_g = \Delta G^{'} \lambda v / V_{got}, \qquad (11)$$

this being of a value of $Z_g = 3.9747x10^{17}$ drops/s. The number of drops that have impacted the rotor blade surface only once (Troyanovsky, 1987) is calculated using the expression:

$$z_{gr} = l_2 b_2 z_{p.r} / \pi \cdot r_{got}^2, \qquad (12)$$

At this point the geometric data of the rotor blade is needed: chord b_2, length l_2 and the number of blades in the crown of the 5th stage and with the data obtained previously, it is observed that $z_{gr} = 1.25x10^{11}$ drops.

The number of drops that have hit the surface of the stator blade only once is obtained from its geometric data: chord b_1, length l_1, the number of blades in the stator of the 5th stage, and z_{ge} is calculated the same as (12) and it is determined that $z_{ge} = 1.537x10^{11}$ drops; in other words, a greater number of drops due to the greater area covered by the stator blades in this special case of the steam turbine. For the calculation of the contact stain velocities of the drop against the surface, and the beginning and duration of extension of the deformed droplet against the surface can be obtained through a particular analysis (Schegliáiev, 1985). First moment of time τ_1, when the drop comes into contact with the surface NN only at the point A_1 does a shock wave arise that propagates in the drop with a velocity $a^{'}$. Simultaneously, the expansion of the stain (in the plane) of contact of the drop in the region of point A_1 takes place.

The velocity c_B with which the points on the circumference of the contact stain move along the impact surface from the point A_1 (Schegliáiev, 1985), is equal to:

$$c_B = w \frac{r_{got}}{r}, \qquad (13)$$

where w is the impact speed of the drop; r_{got} is the radius of the drop; r is the radius of current.

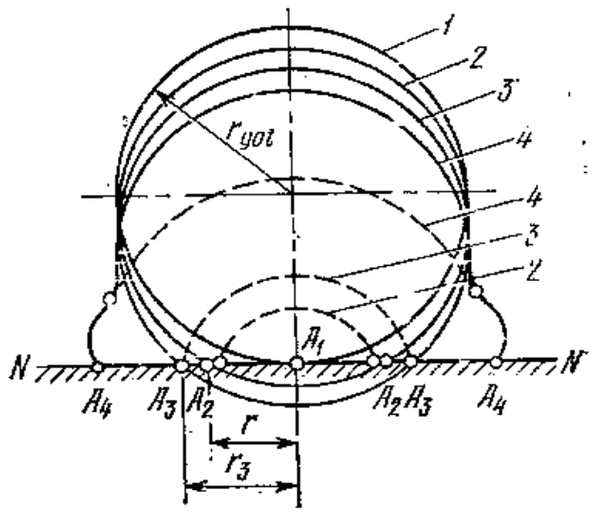

Figura 3 Diagram of the impact of the drop against a flat hard surface NN. _____ drop outlines; ---------- shockwave borders; A_1; A_2A_2; A_3A_3; A_4A_4; borders of the contact staint with the contact surface respectively at the time points $\tau_1, \tau_2, \tau_3, \tau_4$; r_{got} drop radius; r current radius of contact stain; r_3 maximum radius of the contact spot that corresponds to the moment τ_3 of the beginning of the extension (Schegliáiev, 1985).

In the initial period, being small the values of the radius *r*, the velocity c_B exceeds the speed of propagation of the shock wave $a^{'}$. In this case the particles on the surface of the drop come into contact with the impact plane *NN* faster than the propagation of the disturbance inside the drop. In fig. 3 the moment of time τ_2 is shown by the points A_2 which are boundaries of the contact stain. Meanwhile, the shock wave shown by dashed line 2 does not go outside the boundaries of this stain. Only in time τ_3, when the velocity $c_B = a^{'}$, The extension of the drop along the impact surface begins. The boundaries of the contact stain at this point in time are designated by points A_3, and the shock wave by dashed line 3.

ISSN-2531-2189

The posterior extension of the drop ($\tau_4 > \tau_3$) shown with the help of dots A4. The maximum radius of the contact stain r_3 which corresponds to the moment τ_3 of the beginning of the extension (Heinz, 1996), is determined with:

$$r_3 = r_{got}\frac{w}{a'}, \tag{14}$$

While the duration of the time interval in the action period in which the elastic deformation of the drop takes place (Schegliáiev, 1985), can be calculated by means of the equation:

$$\tau_3 - \tau_1 = \frac{wr_{got}}{2(a')^2}. \tag{15}$$

The time in which the impulse acts ($\tau_3 - \tau_1$), is proportional to the impact velocity and the size of the drop. Therefore, according to the above analysis, it can find the contact stain velocity c_B from (13), for radii smaller than the maximum radius, as explained, due to the initial period, and calculating with starting radii of $r_p = 0.1\eta m$, $1\eta m$, $2\eta m$, then, it have to:

$$r_p = 0.1\eta m \quad \Rightarrow \quad c_B = 11{,}600\frac{m}{s},$$

$$r_p = 1\eta m \quad \Rightarrow \quad c_B = 1160\frac{m}{s},$$

$$r_p = 2\eta m \quad \Rightarrow \quad c_B = 580\frac{m}{s}.$$

To determine the extension of the drop along the contact surface r_e, as mentioned above, it arises only when the velocity $c_B = a'$ starts the extension of the drop along the impact surface.

Therefore, from (13) it have:

$$r_{ext} = r_{got}\frac{w}{c_B(=a')}, \tag{16}$$

Then, $r_{ext} = 2.725\mu m$.

The maximum radius r_3 of the stain corresponds to the moment τ_3 of the beginning of the extension. From (14) we find that r^3 = 2.725 μm. For the calculation of the time interval τ the magnitude of all the necessary variables is already available.

Therefore,

$$\tau = \tau_3 - \tau_1 = \frac{w \cdot r_{got}}{2(a')^2}, \tag{17}$$

Then, the time interval in which the deformation of the drop takes place is $\tau = 0.32x10^{-8}\,s$. The time is very small, relatively, since the time of a drop of 100 μm is approximately $\tau = (1...1.5)x10^{-8}$ s. The impact frequency (Troyanovsky, 1987) is determined by the equation:

$$n_y = 0.1\frac{O_1 z_{p.e.} y\varphi^2(1-\rho_{per})^{3/2}v}{b_2 z_{p.r}\sigma x_{per}^3 \upsilon'}u_{per}^3, \tag{18}$$

The frequency of impacts will depend, in addition to physical and design variables, on the quality of the steam in the stage, with humidity in the last stage being approximately 14%, and υ' being the specific volume of saturated steam in the 5th stage; and with the magnitudes already calculated, $n_y \approx 136{,}400$ drops/s are found.

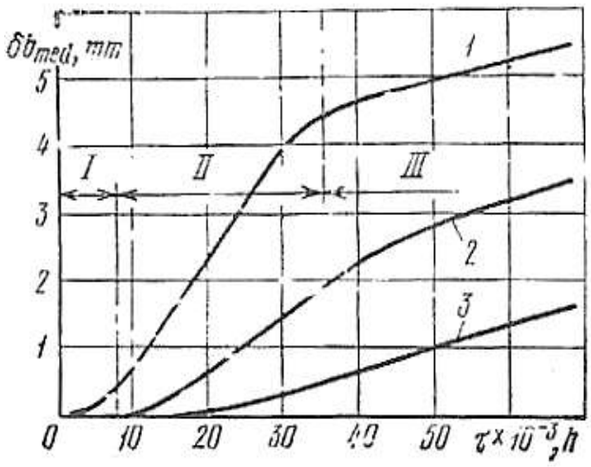

Figura 4 Erosion of the leading edges of the blades as a function of time: 1 – for the last stage of the turbine; 2 – for the penultimate stage; 3 – for the third stage counting from the start [3]

Although the velocity with which the blade mass is reduced does not remain constant over time, the average relative velocity of destruction by erosion is found to be equal to the decrease in volume suffered by the blade material in a unit of time, with with respect to the initial volume, being the destruction of the metal by fatigue, as a result of the action of the impact of the drops and of quadratic dependence between the deformation and the impulse pressure during the impact of the drops. It is determined (Troyanovsky, 1987) as:

ISSN-2531-2189

$\dot{m} = k(\Delta p)^2 n_y$ = 3.36 x 10^{-14} m^3/s, (19)

where *k* is the constant that determines the value of the equation, since *k* is a function of all the properties of the metal of the blades or of the protective layer on the surface of the last one, being, therefore, different for each turbine section, and the type of turbine being analyzed in the calculations.

It is possible, however, to calculate the level of erosion from a graph shown in fig. 4, which relates the operating time against wear caused by erosion on the blade, from the selected stage, observing regular measurements of δ_b = 18 mm on the leading edge of the peripheral zone in the last stage of the low pressure section, over 100,000 hours of average work, locating an erosive level of grade III, estimated for review.

Conclusions

According to the flow conditions and the type of design of the outlet stage of the low pressure section of a 300 MW turbine: 136,400 droplets/s of 4µm radius impacting at 425 m/s on the leading edge of the the rotor blades, determined a wear of 18 mm depth, which is confirmed with the mass loss records of the blades. These parameters influenced the mechanical type erosion, and lead to the investigation of the prevention of the erosion of the blades in the low pressure section or, at least, to control it, since for the field of research and experimentation It is necessary to have a better understanding of the role played by variables at the micro level, as well as macroscopic ones, that cause the origin of humidity.

References

[1] Turbinas de Vapor y de Gas de las Centrales Nucleoeléctricas. B. M. Troyanovski, G. A. Filippov, A. E. Bulkin. Editorial Mir Moscú., 1987.

[2] Turbinas de Vapor. La Teoría del Proceso Térmico y las Construcciones de Turbinas. Parte 1. A.V. Schegliáiev. Editorial Mir Moscú. 1985.

[3] Guía Práctica para la Tecnología de las Turbinas de Vapor. Heinz P. Bloch. Mc Graw Hill, 1996.

[4] Introducción al Diseño Aerodinámico de Compresores Centrífugos y Axiales. Zurita Ugalde V. J. Apuntes académicos SEPI-ESIME-IPN. 1996.

ISSN-2531-2189

Article **Journal of Mechanical Engineering**
December, 2022 Vol.6 No.18 15-20

Characterization of the relationship soil density and simple compression resistance of silty soils

Caracterización de la relación entre la densidad y la resistencia a la compresión simple de limos

RUIZ-CHÁVEZ, Felipe de Jesús†, GUTIÉRREZ-VILLALOBOS, José Marcelino* and ARROYO, Hiram

Universidad de Guanajuato Campus Celaya-Salvatierra, Av. Javier Barros Sierra 201 Col. Ejido de Santa María del Refugio C.P. 38140 Celaya, Gto. México

ID 1st Author: *Felipe De Jesús, Ruiz-Chávez* / **ORC ID**: 0000-0001-7164-6501, **CVU CONACYT ID**: 1239555

ID 1st Co-author: *José Marcelino, Gutiérrez-Villalobos* / **ORC ID**: 0000-0001-5947-1489, **CVU CONACYT ID**: 173461

ID 2nd Co-author: *Hiram, Arroyo* / **ORC ID**: 0000-0002-8343-698X, **CVU CONACYT ID**: 349586

DOI: 10.35429/JME.2022.18.6.15.20 Received: June 30, 2022; Accepted: December 20, 2022

Abstract

The unconfined compressive strength of soils is closely related to the shear strength that soil particles show in a material sample subjected to stress states where there are no lateral restrictions to stabilize the geotechnical structure. It is known that the resistance of a soil depends on its density and the type of soil. In engineering practice, it is highly desirable to have information in the form of empirical relationships that correlate readily and cheaply obtainable data for soil strength. This article presents an experimental study on materials subjected to compression without confinement and that leads to an empirical proposal that relates the density of a soil with the relationship it exhibits to simple compression.

Simple compression, Empirical relations, Density

Resumen

La resistencia a la compresión no confinada de los suelos está íntimamente relacionada con la resistencia al esfuerzo cortante que ofrecen las partículas de suelo en una muestra de material sujeta a estados de esfuerzo donde no existen restricciones laterales que estabilicen la estructura geotécnica. Es reconocido que la resistencia de un suelo depende de su densidad y del tipo de suelo. En la práctica ingenieril es altamente deseable contar con información en forma de relaciones empíricas que correlacionen datos obtenibles de manera rápida y económica para obtener la resistencia del suelo. En este artículo se presenta un estudio experimental sobre materiales sometidos a compresión sin confinamiento y que derivan en una propuesta empírica que relaciona la densidad de un suelo con la relación que exhibe a la compresión simple.

Compresión Simple, Relación empírica, Densidad

Citation: RUIZ-CHÁVEZ, Felipe de Jesús, GUTIÉRREZ-VILLALOBOS, José Marcelino and ARROYO, Hiram. Characterization of the relationship soil density and simple compression resistance of silty soils. Journal of Mechanical Engineering. 2022. 6-17: 15-20

† Researcher contributing as first author.

Introduction

Shear resistance is the fundamental property of soils that is taken into account when designing any geotechnical structure (Rojas *et al*., 2011). A typical experimental observation of soils as construction materials, is that the strength to shear stresses of these materials depends on the confinement stress to which they are subjected (Alonso *et al*., 1990).

To represent this property, the usual convention in soil mechanics is to express the vertical compression stresses with the notation σ_1, as well as the horizontal compression stresses with the notation σ_3. Therefore, the shear stress resistance for a soil sample subjected to a horizontal confining stress σ_3 is expressed by Equation (1):

$$\tau = \sigma_3 \tan\phi + c \quad (1)$$

Where τ is the shear strength exhibited by the soil, ϕ is the friction angle and c is known as cohesion, which is a parameter that depends on moisture conditions.

Under field conditions in which geotechnical structures are not confined, the condition $\sigma_3 = 0$ is met. This state of stress is known as "unconfined" and is present in a variety of geotechnical schemes. Such is the case of vertical cuts in excavations without casings or lateral retention structures. In such a case, the strength of the structure made with soil will depend exclusively on the strength to shear stress quantified as cohesion (Lu *et al*., 2017):

$$\tau = c \quad (2)$$

Therefore, Equation (2) allows identifying the shear strength of soils under unconfined conditions. As can be seen in the Mohr's circle corresponding to the stress state in unconfined compression conditions (Figure 1), this implies that the shear strength in "unconfined" conditions can be evaluated as $\tau = c = \sigma_1/2$. In this case, the stress σ_1 is known as the deviator stress q and has the same value as σ_1.

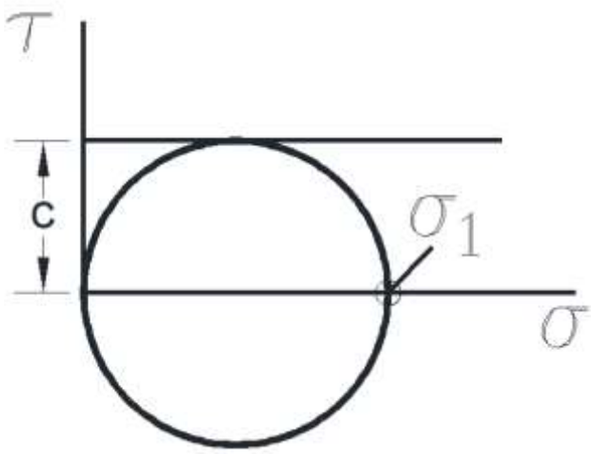

Figure 1 Mohr's circle corresponding to an unconfined stress state

It is fundamental to recognize the role that soil density plays in the value that Equation (2) takes. Experimental reports on laboratory soils make it possible to identify that the parameters to describe shear strength of the soils (Equation (1)) is a function of the density of the materials (Rojas *et al*., 2017). Laboratory tests reported by Futai and Almeida (2005) evaluate the strength parameters of a soil deposit at different depths of a residual soil. Here the different values of ϕ and c parameters for different densities are exhibited. That is, as confirmed by the more agglutinated the soil particles are, the greater the strength to shear stress.

In practical geotechnical engineering, the use of empirical relationships is recurrent to expedite the proposed solutions to a given problem. These solutions, despite being highly dependent on the type of test and the material to be used, allow the test results to be initially used in immediate applications without the need to resort to an exhaustive experimentation campaign.

This paper presents the relationship between the density and the strength to simple compression that a silty sand material exhibit. Such relationship has been extensively recognized in several research papers such as Sun *et al*. (2007). The subsequent section describes the triaxial compression equipment used for the evaluation of the mechanical properties of the soils that were selected for analysis. Moreover, the way in which they were selected and subjected to simple compression efforts is explained.

ISSN-2531-2189

Triaxial compression device used in this study

The triaxial compression equipment used in the development of the research is a Triaxial Press with analog triaxial configuration (Figure 2). It is made up of a load frame that is made up of a robust two-column structure, ensuring rigidity for a maximum capacity of 5.1 tons, with a maximum loading speed of 9mm per minute and a maximum deformation of 90mm. It is added with a cell that confines the soil samples within a controlled space. Axial strains are measured with a potentiometric displacement transducer. The force P is transmitted through an external load cell with a capacity of 5.1 tons to apply a vertical axial force $q = P/A$ to a cylindrical soil sample and produce unit strains $\varepsilon = \Delta l/lo$; A is the cross-sectional area to which the stresses q are applied, Δl are the strains in the direction of application of q, and lo is the initial length of the soil sample.

Figure 2 TRIAX 28-WF-4001 Triaxial Press with analog triaxial configuration

The cell and the transducer send signals that are continuously automatically interpreted and recorded, allowing to track the evolution of the axial stress vs. axial deformation.

Classification of the soil used for the investigation

The soil is a highly compressible silt, classified with the notation MH (according to the Unified Soil Classification System (SUCS) (Braja M. Das, 2010)).

Different tests were carried out with different moisture contents, it is sought that the cylindrical soil sample is uniform and that it allows its placement in the compression equipment. From the moisture content variation tests, it is concluded that the best workability results from considering a moisture content of 15%, since in this way the expected manageability and homogeneity conditions are met. Figure 3 shows the material under various moisture conditions.

Figure 1 Upper: MH1 with a 15% moisture content. Central: MH1 with a 20% moisture content. Lower: MH1 with a 30% moisture content.

ISSN-2531-2189

Fabrication of cylindrical soil samples

It is proposed to study the behavior to unconfined compression under increasing densities 13 kN/m^3, 15 kN/m^3 and 17 kN/m^3, all of them under a moisture content of 15%. It should be noted that it was not possible to produce material samples at densities lower than 13 kN/m^3 since the structure and integrity of the soil cylinder were compromised since the sample was too fragile. The cylindrical soil specimens were fabricated using the static compaction process by layers, controlling the speed of application of the load (0.5 millimeters per minute) in the triaxial compression device.

This allowed the repeatability of the process thus ruling out uncertainties inherent to manual compaction. The strain rate was established considering that the material will be subject to undrained conditions.

The final cylindrical specimens are 9.5 centimeters high and appertain a diameter of 5 centimeters. The cylindrical mold meets the necessary dimensions, with an internal diameter of 5 cm and a height of 10 cm, which must be greater than the height of the soil cylinder in order to apply pressure and provide density. proposal (Figure 4).

Figure 2 Soil sample after compaction in the used mold

Figure 5 shows the triaxial compression device with the specimen in position before applying the deformation loads.

Figure 3 A soil sample placed in position in the triaxial compression device

Study of unconfined strength

Figure 6 shows the cylindrical samples after failure, that is, once the shear strength has been reached under unconfined compression conditions. It can be noted that there is a tilted failure in each one of them, which confirms the results reported by Lu *et al*., (2009) in the sense that the strength to shear stress evaluated under unconfined conditions implies the mobilization of shear stress producing a defined failure zone associated to them.

ISSN-2531-2189

Figure 4 Soil samples at different densities γ driven to failure. Upper: γ = 13 kN/m^3; Central: γ = 15 kN/m^3; Right: γ = 17 kN/m^3

Figure 7, Figure 8 and Figure 9 show the mechanical behavior to strength of samples at different densities. To sequences can be distinguished (solid line and dotted line) which show the evolution of the deformations for two identical samples under the same densities. This was done in order to corroborating the results obtained for a sample. It can be seen that in general the two series of values coincide.

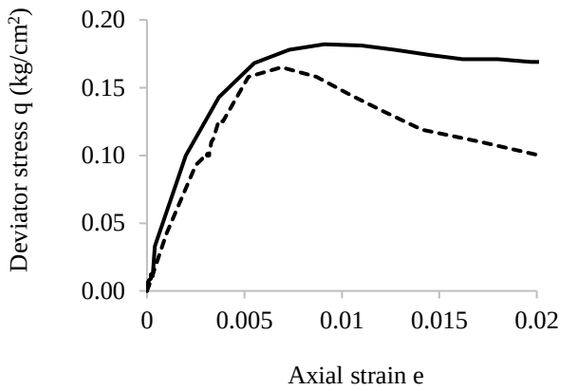

Figure 5 Deviator stress-axial strain relationship for compacted soil samples to $\boldsymbol{\gamma = 13\ kN/m^3}$

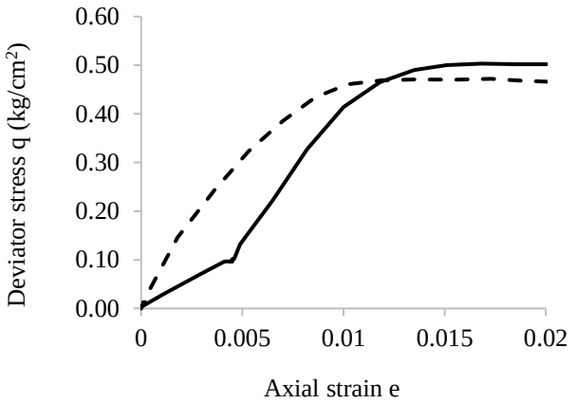

Figure 6 Deviator stress-axial strain relationship for compacted soil samples to $\boldsymbol{\gamma = 15\ kN/m^3}$

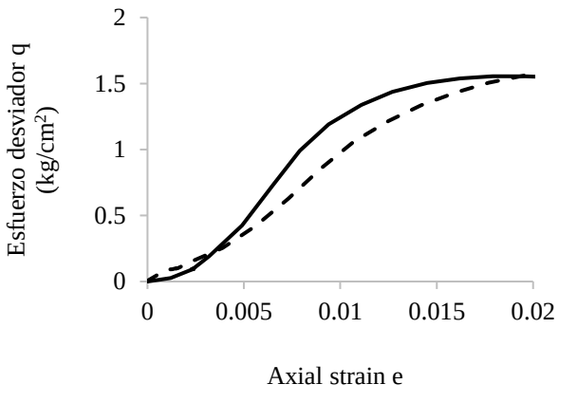

Figura 7 Relación esfuerzo desviador-deformación axial para muestras de suelo compactado a $\boldsymbol{\gamma = 17\ kN/m^3}$

Figure 10 shows the relationship between density and the maximum deviator stress that was sustained. The best fit was retrieved by linear regression, where a clear correlation can be seen between density and unconfined compressive strength, whose equation depicts an exponential nature $q = C_1 e^{C_2}$. It is important to highlight that the tendency of the strength to unconfined compression to decrease, leads to the inference that the material will endure, under the present moisture conditions, shear stresses at densities lower than 7.5 kN/m^3.

ISSN-2531-2189

This coincides with the impediment (in the manufacturing stage of cylindrical soil samples), of fabricating cylindrical samples at densities lower than 10 kN/m^3. On the other hand, there is a rapid growth of strength with density.

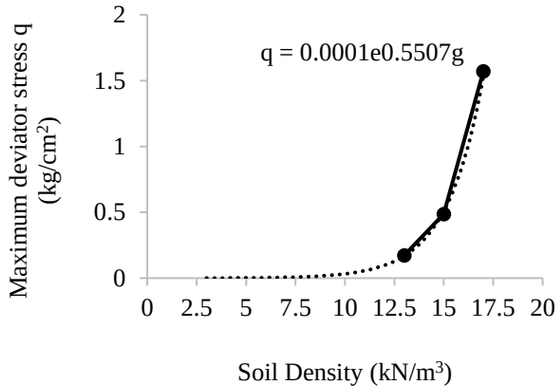

Figura 8 Graphical relationship between soil density and the máximum deviator stress sustained by the samples

Acknowledgement

No funding was required for the present project. Test results were obtained at the soil mechanics laboratory at the University of Guanajuato – Campus Celaya-Salvatierra.

Conclusions

A semi-empirical correlation has been established to relate the density of a silty soil, with its strength in unconfined conditions at constant moisture. This result makes it possible to predict the strength in practical scenarios where geotechnical structures will be subject to unconfined conditions under different densities. The process of fabrication allowed corroborating the results for densities lower than 10 kN/m^3, for which it was not possible to carve the cylindrical soil specimens.

The physical nature of the failure zones in the samples evidences through inclined cracks, the mobilization of shear strength and the consequent strength to these mechanical stresses observed in the soil cylinders that reached the maximum deviator stress.

Future work should consider the behavior of these materials under densities greater than 17 kN/m^3 and at different moisture contents to corroborate the empirical law of variation of material resistance with density.

This empirical law must therefore be calibrated for empirical applications where at least two series of tests must be conducted to calibrate the constants C_1 and C_2 of the linear regression model applicable to these materials.

References

Alonso, E. E., Gens, A., & Josa, A. (1990). *A constitutive model for partially saturated soils* (Vol. 40, Issue 3). https://doi.org/10.1680/geot.1990.40.3.405
Braja M. Das. (2010). *Principles of Foundation Engineering*.

Futai, M. M., and Almeida, M. S. S. (2005). *An experimental investigation of the mechanical behaviour of an unsaturated gneiss residual soil* (Vol. 55, Issue 3). https://doi.org/10.1680/geot.2005.55.3.201

Lu, N., Kim, T.-H., Sture, S., & Likos, W. J. (2009). *Tensile Strength of Unsaturated Sand*. Journal of Engineering Mechanics, 135(12), 1410–1419. https://doi.org/10.1061/(asce)em.1943-7889.0000054

Lu, N., Wu, B., & Tan, C. P. (2017). *Tensile Strength Characteristics of Unsaturated Sands*. https://doi.org/10.1061/ASCE1090-02412007133:2144

Rojas, E., Hurtado, D., Zepeda, A., and María de La Luz Pérez, M. (2011.). *Desplome de un conjunto de edificios. El calvario de un propietario.*

Rojas, E., Chávez, O., Arroyo, H., López-Lara, T., Hernández, J. B., & Horta, J. (2017). *Modeling the Dependency of Soil-Water Retention Curve on Volumetric Deformation*. International Journal of Geomechanics, 17(1). https://doi.org/10.1061/(asce)gm.1943-5622.0000678

Sun, D. A., Sheng, D. C., Cui, H. B., & Sloan, S. W. (2007). *A density-dependent elastoplastic hydro-mechanical model for unsaturated compacted soils*. International Journal for Numerical and Analytical Methods in Geomechanics, 31(11), 1257–1279. https://doi.org/10.1002/nag.579

ISSN-2531-2189

Article **Journal of Mechanical Engineering**
December, 2022 Vol.6 No.18 21-28

Design and manufacture of a splint prototype for the upper extremities of the human body

Diseño y fabricación de prototipo de férula para extremidad superior del cuerpo humano

LICONA-GONZALEZ, Marlon†*, IBARRA-ROBLES, Gabriel Ted, MENTLE-GALINDO, Margarita and BLAS-SANCHEZ, Luis Ángel

Universidad Tecnológica de Xicotepec de Juárez, Mexico

ID 1st Author: *Marlon, Licona-González* / **ORC ID**: 0000-0001-7829-4457, **Researcher ID Thomson**: AAR-6259-2021, **arXiv Author ID**: marlon1987, **CVU CONACYT-ID**: 1138370

ID 1st Co-author: *Gabriel Ted, Ibarra-Robles* / **ORC ID**: 0000-0002-4119-3553, **Researcher ID Thomson**: GXM-8941-2022, **arXiv Author ID**: Gabriel_Ted, **CVU CONACYT ID**: 1257112

ID 2nd Co-autor: *Luis Ángel, Blas-Sánchez* / **ORC ID**: 0000-0003-3313-8551, **Researcher ID Thomson**: AAX-2475-2021, **arXiv Author ID**: AnghelBlas, **CVU CONACYT ID**: 554052

ID 3rd Co-author: *Margarita, Mentle-Galindo* / **ORC ID:** 0000-0001-5390-5960, **Researcher ID Thomson**: S-9202-2018, **arXiv Author ID**: MargaritaG, **CVU CONACYT-ID**: 160164

DOI: 10.35429/JME.2022.18.6.21.28 Received: September 30, 2022; Accepted: December 20, 2022

Abstract

The article presented below shows the process carried out for the elaboration of a splint prototype and the techniques used for its elaboration, the design is carried out with the solidworks software, the designs with the most optimal forms that confer a greater resistance are analyzed. to the prototype, the configuration of the laminating software and the correct orientation for its manufacture are shown. A review of the optimal materials for its manufacture is made, such as PLA, PETG and ABS. For the printing of the prototype, an Ender 3 pro model 3D printing machine will be used, while the Simplify 3D program will be used for the configuration of the printer, which will allow us to configure temperature parameters, such as the extruder temperature, temperature of bed, layer height, printing speed, filling percentage among others.

Splint, Design, ABS, 3D printing

Resumen

El artículo presentado a continuación muestra el proceso llevado a cabo para la elaboración de un prototipo de férula y las técnicas empleadas para su elaboración, el diseño se realiza con el software solidworks, se analizan los diseños con las formas mas óptimas que confieran una mayor resistencia al prototipo, se muestra la configuración del software de laminado y la orientación correcta para su fabricación. Se hace un repaso de los materiales óptimos para su fabricación, como es PLA, PETG y ABS. Para la impresión del prototipo se empleará una máquina de impresión 3D modelo Ender 3 pro mientras que para la configuración de la impresora se hará uso de el programa Simplify 3D, el cual nos permitirá configurar parámetros de temperatura, como la temperatura de extrusor, temperatura de cama, altura de capa, velocidad de impresión, porcentaje de relleno entre otros.

Férula, Diseño, ABS, Impresión 3D

Citation: LICONA-GONZALEZ, Marlon, IBARRA-ROBLES, Gabriel Ted, MENTLE-GALINDO, Margarita, BLAS-SANCHEZ, Luis Ángel. Design and manufacture of a splint prototype for the upper extremities of the human body. Journal of Mechanical Engineering. 2022. 6-18: 21-28

***** Correspondence to the Author (e-mail: marlon.licona@utxicotepec.edu.mx)
† Researcher contributing as first author.

Introduction

A splint is an equipment that is incorporated externally to the body and provides containment, postural correction or deviation, as appropriate. It keeps the body segments in physiological position to perform activities, i.e. aligned, and at the same time allows control of the patient's involuntary movements. [9]

Many of the models that are on sale are not considered entirely practical due to their structure because they tend to be heavy, uncomfortable or very invasive, and many prostheses are rejected because they do not have an aesthetic that the patient considers acceptable [1].

Currently there are different types of injuries, the most common are fractures and/or dislocations. However, the clinical and rehabilitation methods to treat these types of problems have not changed much.

Currently, with the development of new technologies we seek to provide solutions, making use of design software, additive technology equipment, lamination software, 3D scanners, electronics and stress simulation software for the study of materials. This project focuses on the design and development of splints and prostheses that facilitate the user a comfortable rehabilitation without having to limit their mobility.

The variable designs of 3D printed splints allow the establishment of a series of very diverse objectives that help to improve the quality of life of people [4].

Method

Conventional splints, especially those made of plaster, are the most used for the treatment of injuries due to their low cost, but they have a main problem since the user loses strength, mobility and muscle reduction, because they are completely sealed and without ventilation. For the user it tends to be annoying to use this type of splints, since they generate a higher body temperature, sweating and itching in the affected area, having also a greater care in contact with water.

Figure 1 Conventional plaster ferrule
Source: OrthoInfo (October 2022)

The digitized splinting process is promising for the benefit of both clinicians and their patients, provided that future research and investment can overcome the current limitations [5]. For the realization of this work we seek to make an optimal design to subsequently 3D print it by previously making an analysis of the most suitable materials and analyze and the properties of each of them.

The use of additive technology commonly known as 3D printing is not new, but it is only now that with the cheapening of this technology is seeking to provide solutions to problems in different areas ranging from engineering, architecture, medicine etc.

3D printing as a clinical practice is too rare to study and there are no specialized tools for clinical manufacturing practices [3]. Although it is known that 3D printing has been with us for more than 35 years, many are unaware of its use and how interesting this technology can be to find solutions to everyday problems.

Materials

In the market there are several types of plastic materials to be used in the world of 3D printing, among them are the following:

– Pla
– Petg
– Abs
– Nylon
– Carbon Fiber
– Tpu

Each of these materials has particular characteristics, such as:

ISSN-2531-2189

– Flexibility
– Durability
– Chemical Resistance
– Resistance to high temperatures
– Rigidity

For this work, three materials are contemplated, Petg, Abs and Pla: Petg, Abs and Pla, however, ABS confers a higher resistance in terms of stresses such as bending and torsion, these stresses are key for the application of the splint.

SolidWorks software will be used for the development of the splint prototype. We will work together with a physiotherapist specialist to evaluate the preliminary design to ensure that it does not affect the strength of the splint once printed and that it has sufficient ventilation for the user.

The design takes into account three variables for the thickness of the splint ranging from 2mm, 3mm, 4mm, for the first design and printing test will be made three bracelets which are intended to analyze the strength of the material which in this case will be ABS, the length of the bracelets is 10cm with a crescent of 12.5cm.

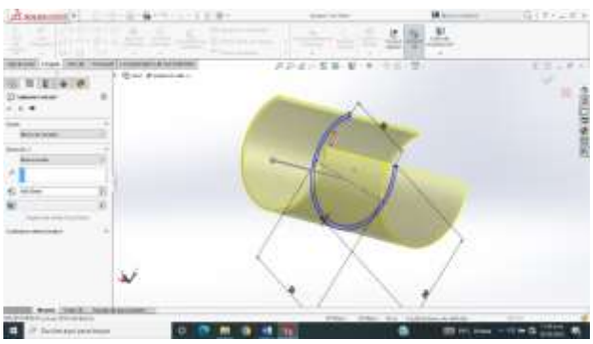

Figure 2 2 mm thick bracelet
Source: Author's contribution (October 2022)

For this first bracelet design a rounding will be applied on the 4 corners with a radius of 20mm.

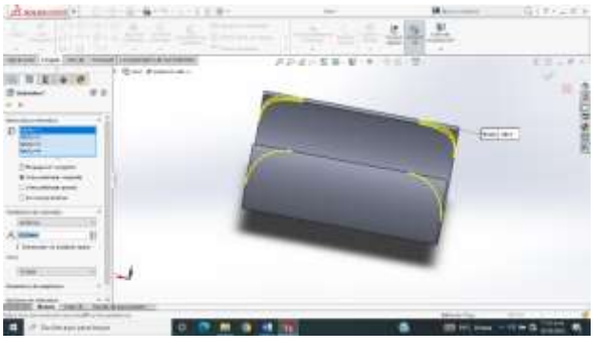

Figure 3 Rounding applied
Source: Author's contribution (October 2022)

Shapes will be inserted to cut-extrude giving only measurements to the holes that will be used as fasteners, subsequently cut and extruded.

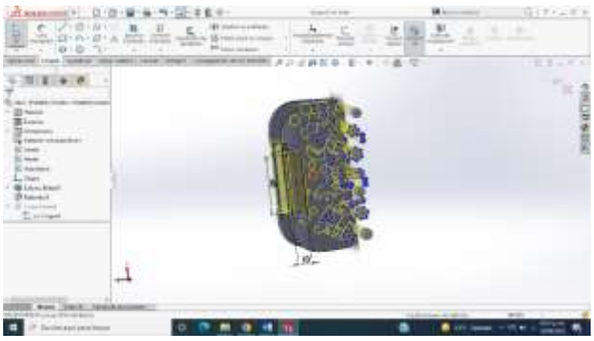

Figure 4 2mm bracelet with extruded shapes
Source: Author contribution (October 2022)

In order to know what would be the ideal thickness, the three bracelets were printed, taking into account the following parameters to configure in the 3D printer:

– Layer height
– Filling percentage
– Temperature
– Speed
– Addition

Based on the above mentioned points, the parameters are as follows:

Parameter	Indicator
Layer height	0.2mm
Percentage of filler	100%
Temperature	235°C
Speed	60 mm/s
Addendum	Balsa

Table 1 Printing Parameters
Source: Author's contribution (October 2022)

ISSN-2531-2189

Once the designs have been finalized and the optimal printing parameters have been analyzed, we proceed to the configuration of the stl, using the Simplify 3D program.

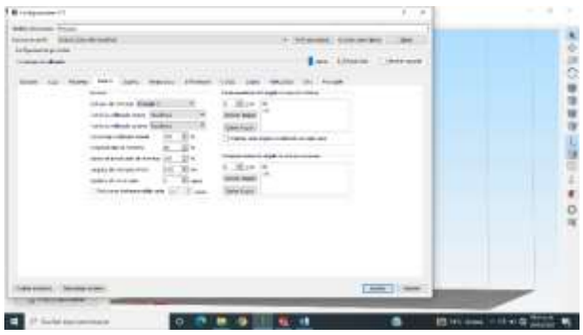

Figure 5 Simplify 3D interface
Source: Author's contribution (October 2022)

Each of the parameters must be entered manually to the laminator, it should be taken into account that if one of the parameters that were set were to change in the laminator, this could cause problems and cause the part once printed to have imperfections and its mechanical properties to decrease. Once the parameters are configured, we proceed to run a simulation of the print in the Simplify 3D program in order to know the following data:

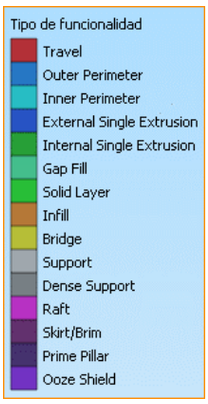

Figure 6 Laminator Color Code
Source: Author's contribution (October 2022)

The simulation run in the laminator shows how the part will be laminated depending on the orientation given, thanks to this we will have an approximate of the time used for printing, as well as the length of the filament needed and its weight.

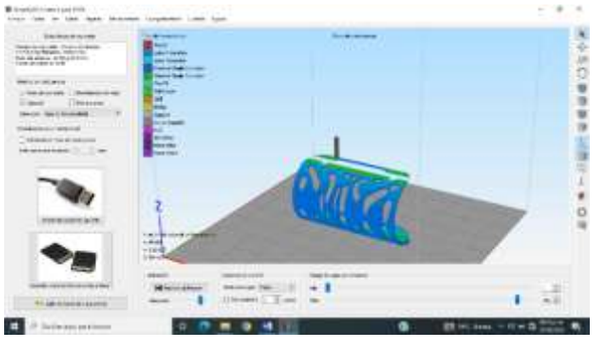

Figure 7 Bracelet Printing Simulation.
Source: Author's contribution (October 2022)

This first bracelet, which has a thickness of 2mm will have a printing time of 2hr 22 min, this time and other data vary depending on the thickness of each one of them, below is a table with the different values obtained in the simulation.

Thickness	Weather	Filament length in meters	Weight
2mm	2hr 22 min	10.2 m	12.56 gr
3mm	3hr 05 min	12.4 m	14.99 gr
4mm	3hr 58 min	14.1 m	16.42 gr

Table 2 Values Obtained in the Simulation
Source: Author's contribution (October 2022)

Once each of the parameters are configured, we proceed to laminate the part, for this work we will use an Ender 3 PRO 3D printer, which has a printing area of 230mm x 230mm x 250mm, these parts will be printed taking into account the parameters presented in Table 1.

Figure 8 Printing of the 2mm cuff on Ender 3 PRO printer
Source: Author's contribution (October 2022)

With the three bracelets printed, we proceed to analyze each one in terms of its resistance and the flexibility needed to open the bracelet so that it can fit correctly in the shape of the forearm.

ISSN-2531-2189

Figure 9 Bracelets of Different Thicknesses
Source: Author's contribution (October 2022)

The cuff with the best results in terms of sufficient opening flexibility was the 3 mm cuff. The following table shows the problems detected in the other cuffs according to the manual bending and compression tests.

Part	Problem
2mm bracelet	Excessive flexibility and easy breakage
4mm bracelet	Lack of flexibility, a greater force is required for opening, which may lead to deformation in the medium term.

Table 3 Problems by Bracelet
Source: Author's contribution (October 2022)

Having already determined the optimal thickness, we proceed to the complete design of the forearm splint, this design will take into account the thickness of 3mm and the shapes will be circular, following the same pattern as the bracelets, the splint will have a height of 20cm.

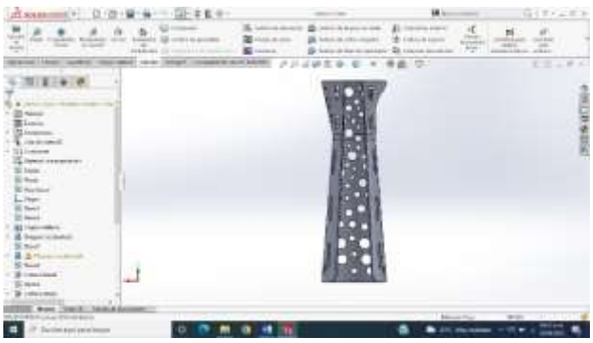

Figure 10 Version 1 splint with circular patterns
Source: Author's contribution (October 2022)

With the design of the first version we proceed to laminate the splint in the Simplify program, the approximate time for the printing of the splint is 6 hr 30 min.

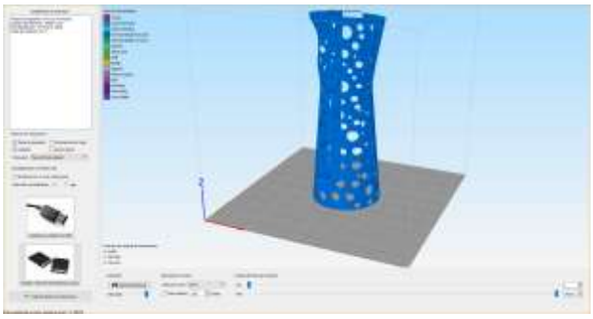

Figure 11 Simulated lamination of Ferrule Version 1
Source: Author's contribution (October 2022)

The configuration used for the ferrule lamination is as follows:

Parameter	Indicator
Layer height	0.15mm
Percentage of filler	100%
Temperature	235°C
Speed	50 mm/s
Addendum	Balsa

Table 4 Impression Parameters Splint V1
Source: Author's contribution (October 2022)

With these parameters we proceed to print this first version of the splint which has as main purpose, to evaluate the design and ergonomics, the total printing time for this version of the splint was 8 hr 23 min,

Problem presented in Version 1

The main problem detected in this first version is the weight which is 200gr, the second problem presented are the shapes of the splint, which are circular and there is not enough space between each one of them which presents the inconvenience that the circles are joined and these minimize its resistance, the third problem are the spaces to secure the splint to the forearm, these spaces are very thin and presented breakages when the securing tapes were placed.

Figure 12 Splint Version 1 Printed
Source: Author's contribution (October 2022)

ISSN-2531-2189

Figure 13 Ferrule Version 1 problems presented
Source: Author's contribution (October 2022)

After this first version and having obtained the first results, a second version of the splint is analyzed and designed, where the aim is to reduce the weight and improve the patterns of the splint, as well as to increase its resistance.

It should never be forgotten that it is the model that is studied and analyzed, and not the real system. From this it is taken into account that the model has to reproduce the behavior of the system in those aspects that are relevant [2].

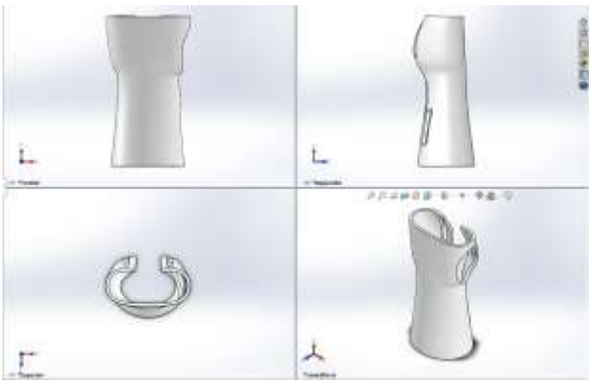

Figure 14 Ferrule Design Version 2
Source: Author's contribution (October 2022)

In order to perform the tests to the design of the splint, the Von Mises analysis was performed with the purpose of demonstrating the stress to which the splint will be subjected with a load of 6N, in this way it can be determined which area of the part is susceptible to suffer a permanent deformation without being able to recover its original shape, complementing this analysis with the displacement and unit deformation analysis.

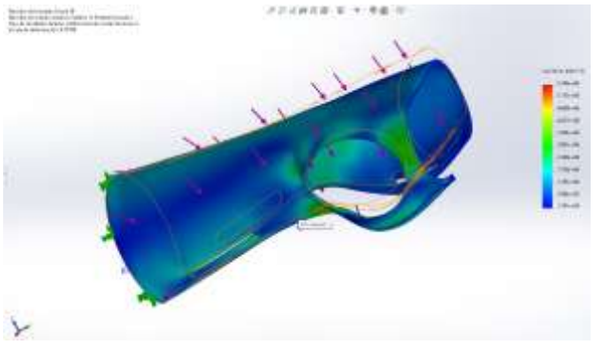

Figure 15 Von Mises analysis
Source: Author's contribution (October 2022)

A displacement analysis was performed with the main objective of showing how many millimeters the splint can be displaced when it is subjected to a load of 6N, resulting in a displacement of 1.891e +00 as shown in Figure 16. This displacement would take place in the lower part of the splint, which is the part most exposed to stress since people regularly rest this part of the body on an object.

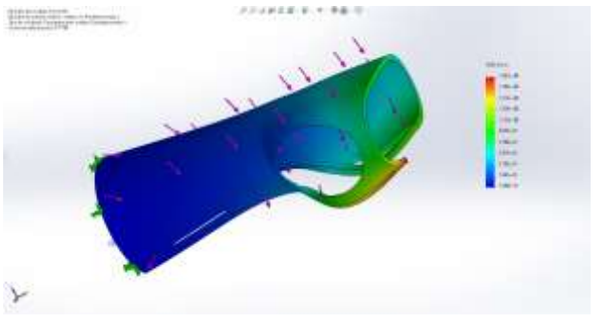

Figure 16 Von Mises analysis
Source: Author's contribution (October 2022)

The design was optimized by reducing the mass percentage by 40% (Figure 17) with respect to the mass of the design in Figure 10, resulting in the optimized design in Figure 18.

Figure 17 Generative design reducing 40% of the mass
Source: Author's contribution (October 2022)

ISSN-2531-2189

Figure 18 Final result of Version 2 splint for impression
Source: Author's contribution (October 2022)

Once the design is concluded and having simulated the different tests, we proceed to the printing of the version 2 splint, for this version the same parameters of table 4 will be used since these presented optimal results for version 1. The approximate printing time for version 2 is 5 hours and 23 minutes with an approximate weight of 53.35 gr, which shows a considerable decrease with respect to the previous design.

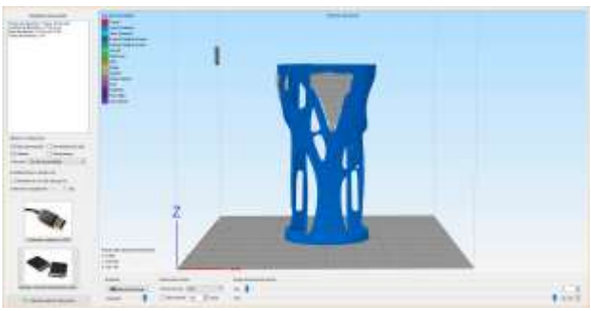

Figure 19 Simulation of Splint Printing Version 2
Source: Author's contribution (October 2022)

Once the printer was configured, we proceeded to print the part, the actual printing time was 5 hours 20 minutes.

Figure 20 Splint Version 2 Printed
Source: Author's contribution (October 2022)

Once the splint is printed, it is placed, and then it will be analyzed with a physiotherapist to evaluate the ergonomics and possible improvements that the splint could have. This work is the first part of three that are scheduled, it is intended to improve the design in the future having already obtained results with a patient, among the future improvements is the placement of electronic devices that can stimulate the patient so that he does not lose mobility. All this will be published in subsequent works.

Conclusion

Designing and manufacturing a piece that is going to be used for the recovery or rehabilitation of a person is a great challenge because it involves an adequate selection of materials, an optimized design that will lead to greater comfort. This first prototype gives us an idea of what can be improved in terms of design and the most appropriate parameters. Likewise, thanks to these tests we are taking into account the implementation of electronic devices that favor the rehabilitation of the user in a much shorter time.

Acknowledgement

This work was carried out with the sponsorship of the Universidad Tecnológica de Xicotepec de Júarez for the Industrial Maintenance and Petroleum career. We are grateful for the support provided.

References

[1] Armijos, E. V. (2022). Fabricación de una prótesis transradial para infantes impresa en 3D con filamento flexible y pla. Polo del Conocimiento, 7(4), 1222-1231. http://polodelconocimiento.com/ojs/index.php/es DOI: 10.23857/pc. v7i4.3884

[2] Aquino, M., Caicedo, I., Buñay, J., & Pozo, E. (2022). Estudio de diseño óptimo de una férula de miembro inferior con patrones de distintas geometrías. Polo del Conocimiento, 7(7),311-339. http://polodelconocimiento.com/ojs/index.php/es DOI: 10.23857/pc. v7i7.4227

[3] Hofmann, M., Williams, K., Kaplan, T., Valencia, S., Hann, G., Hudson, S. E., ... & Carrington, P. (2019, May). " Occupational Therapy is Making" Clinical Rapid Prototyping and Digital Fabrication. In Proceedings of the 2019 CHI Conference on Human Factors in Computing Systems (pp. 1-13). https://doi.org/10.1145/3290605.3300544

[4] Ortega Lázaro, A. (2019). Desarrollo de férulas para impresión 3D: Fase de digitalización y diseño CAD. http://uvadoc.uva.es/handle/10324/36788

[5] Paterson, A. M., Donnison, E., Bibb, R. J., & Ian Campbell, R. (2014). Computer-aided design to support fabrication of wrist splints using 3D printing: A feasibility study. Hand Therapy, 19(4), 102-113. https://doi.org/10.1177/1758998314544802

[6] Patiño Gutiérrez, S. N. Diseño del modelo de un dispositivo soft-robotics para rehabilitación del movimiento de pinza trípode estático de la mano humana (Doctoral dissertation, Universidad Nacional de Colombia). https://repositorio.unal.edu.co/bitstream/handle/unal/82342/1023923777.2022.pdf?sequence=6&isAllowed=y

[7] Pazmiño-Armijos, A. O., Medina-Quintero, E. H., Jácome-Tinoco, J. R., & Pazmiño- https://www.polodelconocimiento.com/ DOI: 10.23857/pc.v7i4.3884

[8] Ramírez González, J. C., & Guyumus Pancho, S. A. Desarrollo de un sistema integral para validación de dispositivos de apoyo durante la marcha humana. http://hdl.handle.net/10554/62005

[9] Bangher, M. C., Abraham, L., Cangini, G., Vecchietti Doldán, M. J., Banda Rabah, R., Petrolini, G., ... & Garbayo del Pino, R. (2020). Órtesis y prótesis: herramientas para la rehabilitación. https://hdl.handle.net/11185/5534

ISSN-2531-2189

[Title in Times New Roman and Bold No. 14 in English and Spanish]

Surname (IN UPPERCASE), Name 1st Author†*, Surname (IN UPPERCASE), Name 1st Coauthor, Surname (IN UPPERCASE), Name 2nd Coauthor and Surname (IN UPPERCASE), Name 3rd Coauthor

Institutional Affiliation of Author including Dependency (No.10 Times New Roman and Italic)

International Identification of Science - Technology and Innovation

ID 1st author: (ORC ID - Researcher ID Thomson, arXiv Author ID - PubMed Author ID - Open ID) and CVU 1st author: (Scholar-PNPC or SNI-CONACYT) (No.10 Times New Roman)

ID 1st coauthor: (ORC ID - Researcher ID Thomson, arXiv Author ID - PubMed Author ID - Open ID) and CVU 1st coauthor: (Scholar or SNI) (No.10 Times New Roman)

ID 2nd coauthor: (ORC ID - Researcher ID Thomson, arXiv Author ID - PubMed Author ID - Open ID) and CVU 2nd coauthor: (Scholar or SNI) (No.10 Times New Roman)

ID 3rd coauthor: (ORC ID - Researcher ID Thomson, arXiv Author ID - PubMed Author ID - Open ID) and CVU 3rd coauthor: (Scholar or SNI) (No.10 Times New Roman)

(Report Submission Date: Month, Day, and Year); Accepted (Insert date of Acceptance: Use Only ECORFAN)

Abstract (In English, 150-200 words)

Objectives
Methodology
Contribution

Abstract (In Spanish, 150-200 words)

Objectives
Methodology
Contribution

Keywords (In English)

Indicate 3 keywords in Times New Roman and Bold No. 10

Keywords (In Spanish)

Indicate 3 keywords in Times New Roman and Bold No. 10

Citation: Surname (IN UPPERCASE), Name 1st Author, Surname (IN UPPERCASE), Name 1st Coauthor, Surname (IN UPPERCASE), Name 2nd Coauthor and Surname (IN UPPERCASE), Name 3rd Coauthor. Paper Title. Journal of Mechanical Engineering. Year 1-1: 1-11 [Times New Roman No.10]

* Correspondence to Author (example@example.org)
† Researcher contributing as first author.

Introduction

Text in Times New Roman No.12, single space.

General explanation of the subject and explain why it is important.

What is your added value with respect to other techniques?

Clearly focus each of its features

Clearly explain the problem to be solved and the central hypothesis.

Explanation of sections Article.

Development of headings and subheadings of the article with subsequent numbers

[Title No.12 in Times New Roman, single spaced and bold]

Products in development No.12 Times New Roman, single spaced.

Including graphs, figures and tables-Editable

In the article content any graphic, table and figure should be editable formats that can change size, type and number of letter, for the purposes of edition, these must be high quality, not pixelated and should be noticeable even reducing image scale.

[Indicating the title at the bottom with No.10 and Times New Roman Bold]

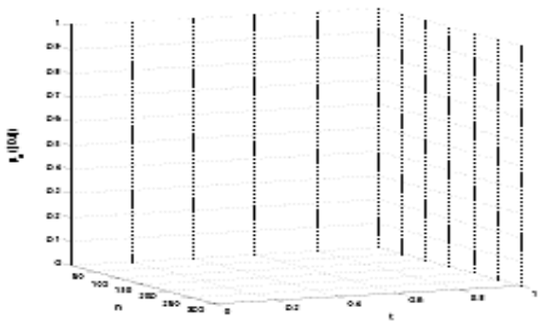

Graphic 1 Title and *Source (in italics)*

Should not be images-everything must be editable.

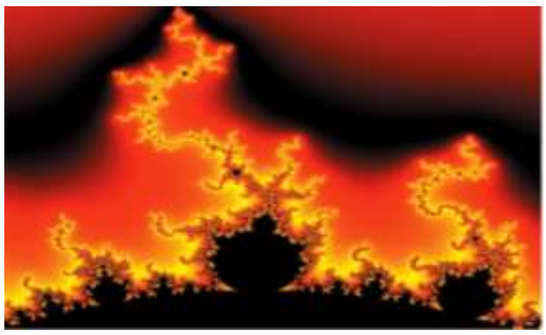

Figure 1 Title and *Source (in italics)*

Should not be images-everything must be editable.

Table 1 Title and *Source (in italics)*

Should not be images-everything must be editable.

Each article shall present separately in **3 folders**: a) Figures, b) Charts and c) Tables in .JPG format, indicating the number and sequential Bold Title.

For the use of equations, noted as follows:

$$Y_{ij} = \alpha + \sum_{h=1}^{r} \beta_h X_{hij} + u_j + e_{ij} \quad (1)$$

Must be editable and number aligned on the right side.

Methodology

Develop give the meaning of the variables in linear writing and important is the comparison of the used criteria.

Results

The results shall be by section of the article.

Annexes

Tables and adequate sources

Thanks

Indicate if they were financed by any institution, University or company.

ISSN 2531-2189

Conclusions

Explain clearly the results and possibilities of improvement.

References

Use APA system. Should not be numbered, nor with bullets, however if necessary numbering will be because reference or mention is made somewhere in the Article.

Use Roman Alphabet, all references you have used must be in the Roman Alphabet, even if you have quoted an Article, book in any of the official languages of the United Nations (English, French, German, Chinese, Russian, Portuguese, Italian, Spanish, Arabic), you must write the reference in Roman script and not in any of the official languages.

Technical Specifications

Each article must submit your dates into a Word document (.docx):

Journal Name
Article title
Abstract
Keywords
Article sections, for example:

1. Introduction
2. Description of the method
3. Analysis from the regression demand curve
4. Results
5. Thanks
6. Conclusions
7. References

Author Name (s)
Email Correspondence to Author
References

Intellectual Property Requirements for editing:

-Authentic Signature in Color of Originality Format Author and Coauthors

-Authentic Signature in Color of the Acceptance Format of Author and Coauthors

-Authentic Signature in Color of the Conflict of Interest Format of Author and Co-authors.

ISSN 2531-2189

Reservation to Editorial Policy

Journal of Mechanical Engineering reserves the right to make editorial changes required to adapt the Articles to the Editorial Policy of the Research Journal. Once the Article is accepted in its final version, the Research Journal will send the author the proofs for review. ECORFAN® will only accept the correction of errata and errors or omissions arising from the editing process of the Research Journal, reserving in full the copyrights and content dissemination. No deletions, substitutions or additions that alter the formation of the Article will be accepted.

Code of Ethics - Good Practices and Declaration of Solution to Editorial Conflicts

Declaration of Originality and unpublished character of the Article, of Authors, on the obtaining of data and interpretation of results, Acknowledgments, Conflict of interests, Assignment of rights and Distribution

The ECORFAN-Mexico, S.C Management claims to Authors of Articles that its content must be original, unpublished and of Scientific, Technological and Innovation content to be submitted for evaluation.

The Authors signing the Article must be the same that have contributed to its conception, realization and development, as well as obtaining the data, interpreting the results, drafting and reviewing it. The Corresponding Author of the proposed Article will request the form that follows.

Article title:

– The sending of an Article to Journal of Mechanical Engineering emanates the commitment of the author not to submit it simultaneously to the consideration of other series publications for it must complement the Format of Originality for its Article, unless it is rejected by the Arbitration Committee, it may be withdrawn.

– None of the data presented in this article has been plagiarized or invented. The original data are clearly distinguished from those already published. And it is known of the test in PLAGSCAN if a level of plagiarism is detected Positive will not proceed to arbitrate.

– References are cited on which the information contained in the Article is based, as well as theories and data from other previously published Articles.

– The authors sign the Format of Authorization for their Article to be disseminated by means that ECORFAN-Mexico, S.C. In its Holding Spain considers pertinent for disclosure and diffusion of its Article its Rights of Work.

– Consent has been obtained from those who have contributed unpublished data obtained through verbal or written communication, and such communication and Authorship are adequately identified.

– The Author and Co-Authors who sign this work have participated in its planning, design and execution, as well as in the interpretation of the results. They also critically reviewed the paper, approved its final version and agreed with its publication.

– No signature responsible for the work has been omitted and the criteria of Scientific Authorization are satisfied.

– The results of this Article have been interpreted objectively. Any results contrary to the point of view of those who sign are exposed and discussed in the Article.

Copyright and Access

The publication of this Article supposes the transfer of the copyright to ECORFAN-Mexico, SC in its Holding Spain for its Journal of Mechanical Engineering, which reserves the right to distribute on the Web the published version of the Article and the making available of the Article in This format supposes for its Authors the fulfilment of what is established in the Law of Science and Technology of the United Mexican States, regarding the obligation to allow access to the results of Scientific Research.

Article Title:

Name and Surnames of the Contact Author and the Coauthors	Signature
1.	
2.	
3.	
4.	

Principles of Ethics and Declaration of Solution to Editorial Conflicts

Editor Responsibilities

The Publisher undertakes to guarantee the confidentiality of the evaluation process, it may not disclose to the Arbitrators the identity of the Authors, nor may it reveal the identity of the Arbitrators at any time.

The Editor assumes the responsibility to properly inform the Author of the stage of the editorial process in which the text is sent, as well as the resolutions of Double-Blind Review.

The Editor should evaluate manuscripts and their intellectual content without distinction of race, gender, sexual orientation, religious beliefs, ethnicity, nationality, or the political philosophy of the Authors.

The Editor and his editing team of ECORFAN® Holdings will not disclose any information about Articles submitted to anyone other than the corresponding Author.

The Editor should make fair and impartial decisions and ensure a fair Double-Blind Review.

Responsibilities of the Editorial Board

The description of the peer review processes is made known by the Editorial Board in order that the Authors know what the evaluation criteria are and will always be willing to justify any controversy in the evaluation process. In case of Plagiarism Detection to the Article the Committee notifies the Authors for Violation to the Right of Scientific, Technological and Innovation Authorization.

Responsibilities of the Arbitration Committee

The Arbitrators undertake to notify about any unethical conduct by the Authors and to indicate all the information that may be reason to reject the publication of the Articles. In addition, they must undertake to keep confidential information related to the Articles they evaluate.

Any manuscript received for your arbitration must be treated as confidential, should not be displayed or discussed with other experts, except with the permission of the Editor.

The Arbitrators must be conducted objectively, any personal criticism of the Author is inappropriate.

The Arbitrators must express their points of view with clarity and with valid arguments that contribute to the Scientific, Technological and Innovation of the Author.

The Arbitrators should not evaluate manuscripts in which they have conflicts of interest and have been notified to the Editor before submitting the Article for Double-Blind Review.

Responsibilities of the Authors

Authors must guarantee that their articles are the product of their original work and that the data has been obtained ethically.

Authors must ensure that they have not been previously published or that they are not considered in another serial publication.

Authors must strictly follow the rules for the publication of Defined Articles by the Editorial Board.

The authors have requested that the text in all its forms be an unethical editorial behavior and is unacceptable, consequently, any manuscript that incurs in plagiarism is eliminated and not considered for publication.

Authors should cite publications that have been influential in the nature of the Article submitted to arbitration.

Information services

Indexation - Bases and Repositories

LATINDEX (Scientific Journals of Latin America, Spain and Portugal)
EBSCO (Research Database - EBSCO Industries)
RESEARCH GATE (Germany)
GOOGLE SCHOLAR (Citation indices-Google)
MENDELEY (Bibliographic References Manager)
REDIB (Ibero American Network of Innovation and Scientific Knowledge - CSIC)
HISPANA (Information and Bibliographic Orientation-Spain)

Publishing Services

Citation and Index Identification H
Management of Originality Format and Authorization
Testing Article with PLAGSCAN
Article Evaluation
Certificate of Double-Blind Review
Article Edition
Web layout
Indexing and Repository
ArticleTranslation
Article Publication
Certificate of Article
Service Billing

Editorial Policy and Management

38 Matacerquillas, CP-28411. Moralzarzal –Madrid-España. Phones: +52 1 55 6159 2296, +52 1 55 1260 0355, +52 1 55 6034 9181; Email: contact@ecorfan.org www.ecorfan.org

Journal of Mechanical

"Behavior analysis of a hydraulic circuit through a low-cost data acquisition system"
CERVANTES-ÁLVAREZ, Francisco Andrés, LÓPEZ-OLMOS, Fabrizio, TORRES-DEL CARMEN, Felipe de Jesús and CAPILLA-GONZÁLEZ, Gustavo
Universidad de Guanajuato

"Determination of Physical parameters that contribute to the erosion of rotor blades in a steam turbine"
RUEDA-MARTINEZ, Fernando, GARRIDO-MELÉNDEZ, Javier, MENDOZA-GONZÁLEZ, Felipe and RODRÍGUEZ-GARCÍA, Ernesto R.
Universidad Veracruzana

"Characterization of the relationship soil density and simple compression resistance of silty soils"
RUIZ-CHÁVEZ, Felipe de Jesús, GUTIÉRREZ-VILLALOBOS, José Marcelino and ARROYO, Hiram
Universidad de Guanajuato

"Design and manufacture of a splint prototype for the upper extremities of the human body"
LICONA-GONZALEZ, Marlon, IBARRA-ROBLES, Gabriel Ted, MENTLE-GALINDO, Margarita and BLAS-SANCHEZ, Luis Ángel
Universidad Tecnológica de Xicotepec de Juárez

2531-2189
ISSN 2531-2189

www.ecorfan.org